Testing turbulent closure models with convection simulations

J. E. Snellman[1], **P. J. Käpylä**[1,2,3], **M. J. Käpylä**[3,1,2], **M. Rheinhardt**[1,2], and **B. Dintrans**[4]

[1] Department of Physics, Gustaf Hällströmin katu 2a (PO Box 64), FI-00014 University of Helsinki, Finland
[2] NORDITA, Roslagstullsbacken 23, SE-10691 Stockholm, Sweden
[3] ReSoLVE Centre of Excellence, Department of Information and Computer Science, Aalto University, PO Box 15400, FI-00076 Aalto, Finland
[4] Observatoire Midi-Pyrénées, Laboratoire d'Astrophysique de Toulouse-Tarbes (UMR5572), 14 Avenue Edouard Belin, 31400 Toulouse, France

The dates of receipt and acceptance should be inserted later

Key words hydrodynamics – turbulence – convection – Sun: rotation – stars: rotation

We compare simple analytical closure models of homogeneous turbulent Boussinesq convection for stellar applications with three–dimensional simulations. We use turbulent closure models to compute the fluxes of angular momentum and heat as a function of rotation rate measured by the Taylor number. We also investigate cases with varying angles between the angular velocity and gravity vectors, corresponding to locating the computational domain at different latitudes ranging from the pole to the equator of the star. We perform three–dimensional numerical simulations in the same parameter regimes for comparison. The free parameters appearing in the closure models are calibrated by two fitting methods using simulation data. Unique determination of the closure parameters is possible only in the non–rotating case or when the system is placed at the pole. In the other cases the fit procedures yield somewhat differing results. The quality of the closure is tested by substituting the resulting coefficients back into the closure model and comparing with the simulation results. To eliminate the possibilities that the results obtained depend on the aspect ratio of the simulation domain or suffer from too small Rayleigh numbers we performed runs varying these parameters. The simulation data for the Reynolds stress and heat fluxes broadly agree with previous compressible simulations. The closure works fairly well with slow and fast rotation but its quality degrades for intermediate rotation rates. We find that the closure parameters depend not only on rotation rate but also on latitude. The weak dependence on Rayleigh number and on the aspect ratio of the domain indicates that our results are generally valid.

1 Introduction

Turbulent convection is responsible for the transport of angular momentum and heat in stellar convection zones, in particular in that of the Sun. In combination with global rotation, these turbulent flows lead to the generation of large–scale differential rotation and meridional circulation (e.g. Rüdiger 1989), which on the other hand, play key roles in sustaining the dynamo of the Sun (e.g. Krause & Rädler 1980; Rüdiger & Hollerbach 2004).

During the last decades, growing computational resources have allowed direct and large–eddy numerical simulations to reach a level of sophistication where many aspects of the solar differential rotation and dynamo can be captured self–consistently (see, e.g. Ghizaru et al. 2010; Käpylä et al. 2012; Miesch et al. 2006; Miesch & Toomre 2009; Warnecke et al. 2013). However, these simulations are still computationally very expensive and cannot be employed in performing comprehensive parameter surveys. Furthermore, even the currently highest resolution simulations are still far from real stars in parameter space (e.g. Käpylä 2011). An alternate way of dealing with the problem is to parametrize the small scales by turbulent transport coefficients and solve directly only for the large scales. This is often done by approximating higher–order correlations by lower order ones in so–called *closure* approaches. In general the pitfall lies in the limited validity of the analytical approximations under which the results are derived. Hence fine–tuning of the model parameters is usually required.

There have been many different closure models proposed and used through the years in astrophysical convection studies (e.g. Canuto et al. 1996; Canuto 1997, 2011; Garaud et al. 2010; Xiong 1989). These models differ in the approximations used (e.g. whether the fluid is considered incompressible, anelastic, or fully compressible), and in which terms and in what way closure approximations are invoked. For instance, the closure studied in this paper (Garaud et al. 2010), is based on deriving exact time evolution equations for second–order correlations and replacing the therein occurring third–order ones by relaxation terms with a variable relaxation time.

Another widely used model was introduced by Canuto et al. (1996), who started from the evolution equations derived by Yamaguchi (1963) for the spectra of the mean square velocity, mean square temperature perturbation and turbulent heat flux in the Boussinesq approximation. The nonlinear transfer terms corresponding to the triple correlation terms $\langle uuu \rangle$ and $\langle u\theta\theta \rangle$ (in symbolic notation) were then equated to the spectra of mean square vorticity and

mean square temperature gradient, respectively, while the term of the type $\langle uu\theta \rangle$ was assumed to depend on the two other ones. For the closure "parameters", a k-dependent turbulent viscosity and heat conductivity were introduced. These turbulent diffusivities were considered to be related mutually by a single (constant) free parameter. Finally, the turbulent viscosity was set in relation to the mean square vorticity with a coefficient derived from the requirement that in the inertial range the resulting spectrum is to be of Kolmogorov type. In that way, the (normalized) turbulent heat flux, rms value of the velocity, turbulent pressure etc. can be determined explicitly after having chosen the free paramter.

A promising approach to the problem of validating or calibrating turbulent closure models is to compare their results with direct numerical simulations (DNS). Fairly little has been done to accomplish this in the astrophysical context. This is especially true for closures dealing with turbulent convection (see, however, Garaud et al. 2010).

In this paper we build upon previous studies where simple analytical closure models were compared with simulations of forced or magnetorotationally excited turbulence in fully periodic systems (Käpylä & Brandenburg 2008; Liljeström et al. 2009; Snellman et al. 2012a, 2009, 2012b). Here we extend this work to turbulent convection in unstratified Rayleigh–Bénard setups. Our aim is to compare three-dimensional DNS with the closure model for convection put forward by Garaud et al. (2010) (hereafter GOMS10). This closure is an extension of earlier work related to isothermal magnetohydrodynamic turbulence (Ogilvie 2003). The bulk of GOMS10 is devoted to the derivation and calibration of a closure model for a Boussinesq system. Results of DNS and experiments of bounded and hence inhomogeneous non–rotating Rayleigh-Bénard convection are referred to for the purpose of determining the free parameters of the model. They found that in the statistically stationary state, to a certain extent universal constants can be extracted which moreover coincide partly with those from a corresponding study of the clearly different situation of shear flows, see Garaud & Ogilvie (2005).

Similarly, in GOMS10 an additional free parameter of the closure for *homogeneous* non–rotating Rayleigh–Bénard convection was estimated on the basis of DNS results where its universality turned out to be limited by the destabilization of the fluctuations in shallow computational domains. The predictions of the closure model for the same setup, but with rotation included, were set into relation of previous analytical results. However, no direct comparison with corresponding DNS results was performed, in particular, there was no independent calibration of the model parameters.

The emergence of coherent structures covering the whole vertical extent of the domain was quite generally pointed out to be limiting the validity of the essentially *local* closure. For the case of rotating homogeneous Rayleigh-Bénard convection a further limit was found in the independence of the closure model on the rotation rate when gravitation and rotation are perfectly aligned.

Hence, the goal of the present paper is to scrutinize the potential of the homogeneous GOMS10 closure model for *rotating convection*.

2 Models and methods

We consider a closure model for Boussinesq convection in infinitely extended space following Miller & Garaud (2007) and GOMS10.

2.1 The Boussinesq system

2.1.1 Basic equations

In general, the time evolution of the velocity and temperature fields is governed by the Navier-Stokes, continuity, and heat transfer equations

$$\rho \frac{D\boldsymbol{U}}{Dt} = -\boldsymbol{\nabla} p + \rho\,(\boldsymbol{g} - 2\,\boldsymbol{\Omega} \times \boldsymbol{U} + \boldsymbol{f}_{\rm visc}), \quad (1)$$

$$\frac{D \ln \rho}{Dt} = -\boldsymbol{\nabla} \cdot \boldsymbol{U}, \quad (2)$$

$$\rho c_V \frac{DT}{Dt} = \boldsymbol{\nabla} \cdot K \boldsymbol{\nabla} T - p \boldsymbol{\nabla} \cdot \boldsymbol{U} + 2\nu\rho \mathsf{S}^2, \quad (3)$$

where $\boldsymbol{U}$ is the velocity, ρ is the density, and $\boldsymbol{g}$ is the gravitational acceleration, which is assumed constant. $\boldsymbol{f}_{\rm visc}$ is the viscous force per mass, p is the pressure, T is the temperature, and c_V is the specific heat at constant volume, again assumed constant. K is the heat conductivity and $D/Dt = \partial/\partial t + \boldsymbol{U} \cdot \boldsymbol{\nabla}$ denotes the advective derivative. The viscous force is given by

$$\boldsymbol{f}_{\rm visc} = \nu \Big(\boldsymbol{\nabla}^2 \boldsymbol{U} + \tfrac{1}{3} \boldsymbol{\nabla} \boldsymbol{\nabla} \cdot \boldsymbol{U} + 2\,\mathsf{S} \cdot \boldsymbol{\nabla} \ln \rho \Big), \quad (4)$$

with the kinematic viscosity ν, assumed constant. S is the traceless rate of strain tensor, which can be written in component form as

$$\mathsf{S}_{ij} = \tfrac{1}{2}\,(\partial_j U_i + \partial_i U_j) - \tfrac{1}{3} \delta_{ij} \partial_k U_k\,. \quad (5)$$

In the Boussinesq approximation, convection is understood as a perturbation to a stationary, purely conductive reference state with constant density ρ_0 which is hence governed by

$$0 = -\boldsymbol{\nabla} p_0 + \rho_0 \boldsymbol{g}, \quad 0 = \chi \boldsymbol{\nabla}^2 T_0 + q_0, \quad (6)$$

where the thermal diffusivity $\chi = K/\rho_0 c_V$ is assumed constant, and a stationary heat source q_0 is included. In this paper, however, we rely on the simplest case with $q_0 = 0$ and a consequently uniform temperature gradient $\boldsymbol{\nabla} T_0$ enforced by appropriate boundary conditions. Denoting the deviations of density, pressure and temperature from their

reference values caused by convection by ρ', p', and Θ, respectively, that is, $\rho = \rho_0 + \rho'$, $p = p_0 + p'$ and $T = T_0 + \Theta$, we obtain from (1) and (6) for the momentum balance

$$\rho \frac{D\boldsymbol{U}}{Dt} = -\boldsymbol{\nabla} p' + \rho' \boldsymbol{g} - 2\rho \boldsymbol{\Omega} \times \boldsymbol{U} + \rho \boldsymbol{f}_{\rm visc}. \quad (7)$$

According to the key idea of the Boussinesq approximation, the density deviation ρ' from its reference value ρ_0 is assumed to be negligible *except in the buoyancy force* $\rho\boldsymbol{g}$ (see, e.g., Chandrasekhar 1961). Density and temperature perturbations are interconnected by

$$\frac{\varrho'}{\rho_0} = -\alpha(T - T_0) = -\alpha\Theta, \quad (8)$$

where α is the coefficient of thermal volume expansion. Finally, the equations of the Boussinesq approximation read

$$\frac{D\boldsymbol{U}}{Dt} = -\boldsymbol{\nabla}\Psi - \alpha\Theta\boldsymbol{g} - 2\boldsymbol{\Omega} \times \boldsymbol{U} + \nu\boldsymbol{\nabla}^2\boldsymbol{U}, \quad \boldsymbol{\nabla} \cdot \boldsymbol{U} = 0, \quad (9)$$

$$\frac{D\Theta}{Dt} = \chi\boldsymbol{\nabla}^2\Theta - \boldsymbol{U} \cdot \boldsymbol{\nabla} T_0 \,. \quad (10)$$

Here, the reduced pressure $\Psi = p'/\rho_0$ was introduced and the viscous force was simplified for the now incompressible flow.

As first pointed out by Spiegel & Veronis (1960) this reasoning has to be modified when being applied to gases rather than (practically incompressible) liquids: While $\boldsymbol{\nabla} \cdot \boldsymbol{U} = 0$ is retained for the continuity equation and the viscous force, the compression work $-p\boldsymbol{\nabla}\cdot\boldsymbol{U}$ must not simply be omitted in (10). Instead, it gives rise to a twofold correction: For an ideal gas, χ has to be redefined by employing c_p instead of c_V and the background temperature gradient has to be replaced by the difference $\boldsymbol{\nabla} T_0 - \boldsymbol{g}/c_p$ with the adiabatic temperature gradient $\boldsymbol{g}/c_p$. Thus we have

$$\frac{D\Theta}{Dt} = \chi\boldsymbol{\nabla}^2\Theta - \boldsymbol{U} \cdot \left(\boldsymbol{\nabla} T_0 - \frac{\boldsymbol{g}}{c_p}\right), \quad (11)$$

with χ being now defined as $\chi = K/\rho_0 c_p$.

Contributions to the heat budget from viscous heating are omitted in (10), but can easily be taken in to account by restoring the term $2\nu\mathbf{S}^2/c_V$. However, in order to guarantee energy conservation, expansion work has then also to be included in the form of a cooling term $\alpha\Theta\boldsymbol{g} \cdot \boldsymbol{U}$.

2.1.2 Domain, boundary conditions, control parameters

For the computational domain we consider a rectangular box thought of being cut out at a varying latitude from the convection zone of a rotating star. We choose Cartesian coordinates (x, y, z) such that their directions locally correspond to those of the global spherical coordinates (ϑ, ϕ, r) having their axis $\vartheta = 0$ aligned with the angular velocity vector $\boldsymbol{\Omega}$. In the local Cartesian coordinates, the latter then reads

$$\boldsymbol{\Omega} = \Omega_0[-\sin\vartheta, 0, \cos\vartheta], \quad (12)$$

where ϑ is the colatitude. Gravity $\boldsymbol{g}$ is always taken to be radial, that is, to coincide with the local z direction. We place the box at seven different positions defined by varying ϑ in equidistant steps of 15 degrees from 0° (pole) to 90° (equator). For the dimensions of the box, L_x, L_y, L_z, we set $L_x = L_y$ while L_z may be varied, see Section 3.2.4. For all quantities, periodic boundary conditions in all directions are employed throughout the paper. If now the reference temperature gradient $\boldsymbol{\nabla} T_0$ is assumed constant over the box, that is, in the infinite space, it is implied that the turbulence is *homogeneous* (but still anisotropic because gravity and rotation introduce preferred directions). Hence this setup is labelled as *homogeneous Rayleigh-Bénard convection*. We note that this type of a system is not realizable in nature due to the periodic boundaries as discussed in Calzavarini et al. (2006). However, it is particularly useful in testing closure models due to its simplicity.

The system defined by Eqs. (9)–(11) is governed by the following three dimensionless parameters: The magnitude of the temperature gradient (and eventually the vigour of the convection) is quantified by the Rayleigh number

$$\mathrm{Ra} = \frac{\alpha g d^3 (\Delta T_0 - g d/c_p)}{\nu\chi}, \quad (13)$$

where $g = g_z$ and $d = L_z$ is the vertical extent of the domain. In general, ΔT_0 is the reference temperature difference between its top and bottom. For the homogeneous case considered here, the definition (13) has to be modified properly employing the constant effective (= prescribed minus adiabatic) background temperature gradient $G_0 = \nabla_z T_0 - g/c_p$, that is

$$\mathrm{Ra} = \frac{\alpha g d^4 G_0}{\nu\chi}. \quad (14)$$

The ratio of viscosity and thermal diffusivity is given by the Prandtl number

$$\mathrm{Pr} = \frac{\nu}{\chi}, \quad (15)$$

and finally the rotation rate is measured by the Taylor number

$$\mathrm{Ta} = \frac{4\Omega_0^2 d^4}{\nu^2}. \quad (16)$$

Another way to express the strengths of rotation and viscous effects, but in the form of diagnostics rather than of control parameters, is provided by the Coriolis and Reynolds numbers, respectively,

$$\mathrm{Co} = \frac{2\,\Omega_0}{U_{\rm rms} k_{\rm f}}, \quad \mathrm{Re} = \frac{U_{\rm rms}}{\nu k_{\rm f}}, \quad (17)$$

where $k_{\rm f} = 2\pi/d$ is the wave number corresponding to the vertical extent d and $U_{\rm rms} = \langle U^2 \rangle^{1/2}$ is the root mean square velocity where the angle brackets denote averaging over the volume of the domain. The efficiency of the convective heat transfer is measured by the Nusselt number estimating the ratio of the total to the conductive heat flux

$$\mathrm{Nu} = \frac{\langle U_z \Theta \rangle}{\chi G_0} + 1. \quad (18)$$

2.1.3 Closure model

In this section we present the homogenous version of the GOMS10 model. The details of the more general inhomogenous model can be found in Appendix A. First we specify the averaging procedure by which the mean quantities are defined. Given the homogeneity of our model, volume averages are applied to the numerical results throughout this paper. Hence, the mean of a quantity f, indicated by an overbar, is given by

$$\overline{f} = \langle f \rangle = \frac{1}{L_x L_y L_z} \int_{L_z}\int_{L_y}\int_{L_x} f(x,y,z)dxdydz. \quad (19)$$

This procedure satisfies all the Reynolds averaging rules. Denoting fluctuating quantities with lowercase letters, we have $\boldsymbol{U} = \overline{\boldsymbol{U}} + \boldsymbol{u}$, $\Theta = \overline{\Theta} + \theta$ etc. When assuming $\Omega_y = 0$ and the temperature gradient to be defined as a constant vector parallel to gravity $\boldsymbol{g} = g\boldsymbol{e}_z$, hence $\boldsymbol{\nabla} T_0 - \boldsymbol{g}/c_p = G_0 \boldsymbol{e}_z$, the equations for the mean velocity and temperature resulting from (9), (11) read

$$\begin{aligned} \dot{\overline{U}}_x &= 2\Omega_z \overline{U}_y, & \dot{\overline{U}}_y &= -2\Omega_z \overline{U}_x + 2\Omega_x \overline{U}_z, \\ \dot{\overline{U}}_z &= -\alpha g \overline{\Theta} - 2\Omega_x \overline{U}_y, & \dot{\overline{\Theta}} &= -G_0 \overline{U}_z\,, \end{aligned} \quad (20)$$

cf. also (A12), (A13). As a consequence of the chosen average, spatial derivatives vanish and the continuity equation is satisfied automatically. The system (20) does not invoke the Reynolds stress tensor $\boldsymbol{\mathcal{R}} = \{\mathcal{R}_{ij}\} = \{\overline{u_i u_j}\}$, the turbulent heat flux, $\boldsymbol{\mathcal{F}} = \{\mathcal{F}_i\} = \{\overline{\theta u_i}\}$ or the temparature variance $\mathcal{Q} = \overline{\theta^2}$ and is therefore closed. As it is homogeneous, its solutions vanish if the initial conditions do so. But as it possesses unstable solutions for $\alpha g G_0 > 0$, which are artefacts of the homogeneity of the system. We suppress them in the DNS by removing the mean flow at every time step.

Evolution equations for the Reynolds stress and turbulent heat flux can be derived from the equations for the fluctuating quantities $\boldsymbol{u}$ and θ, see Appendices A and B. In doing so one comes inevitably across higher–order correlations of $\boldsymbol{u}$ and θ. The essential step of the closure procedure as proposed in GOMS10 consists then in replacing these correlations by aggregates of second–order correlations, more specifically, of the quantities $\mathcal{R}_{ij}$ and $\mathcal{F}_i$ themselves. In an analogous way, some second–order correlations which cannot directly be expressed by the components of $\boldsymbol{\mathcal{R}}$ and $\boldsymbol{\mathcal{F}}$ are modelled. In order to obtain a closed system, an additional equation for $\mathcal{Q}$ is needed which can be derived using Eq. (11) and which is also subjected to the closure procedure. The details can again be found in Appendix A. Finally, the closed set of equations reads

$$\begin{aligned} &\dot{\mathcal{R}}_{ij} + \alpha(\mathcal{F}_i g_j + \mathcal{F}_j g_i) + 2\Omega_l(\varepsilon_{ilk}\mathcal{R}_{jk} + \varepsilon_{jlk}\mathcal{R}_{ik}) \quad (21) \\ &\quad = -\left(\frac{C_1 + C_2}{L}\mathcal{R}^{1/2} + \nu\frac{C_\nu}{L^2}\right)\mathcal{R}_{ij} + \frac{C_2}{3L}\mathcal{R}^{3/2}\delta_{ij}, \end{aligned}$$

$$\begin{aligned} &\dot{\mathcal{F}}_i + \mathcal{R}_{iz}G_0 + \alpha\mathcal{Q}g_i + 2\varepsilon_{ijk}\Omega_j\mathcal{F}_k \quad (22) \\ &\quad = -\left(\frac{C_6}{L}\mathcal{R}^{1/2} + \tfrac{1}{2}(\nu+\chi)\frac{C_{\nu\chi}}{L^2}\right)\mathcal{F}_i, \end{aligned}$$

$$\dot{\mathcal{Q}} + 2\mathcal{F}_z G_0 = -\left(\frac{C_7}{L}\mathcal{R}^{1/2} + \chi\frac{C_\chi}{L^2}\right)\mathcal{Q}, \quad (23)$$

where $\mathcal{R} = \mathcal{R}_{xx} + \mathcal{R}_{yy} + \mathcal{R}_{zz}$ is the trace of $\boldsymbol{\mathcal{R}}$, $C_{1,2,6,7,\nu,\nu\chi,\chi}$ are the model parameters and L is a characteristic length scale. In the following we will refer to the entirety of these coefficients by C_*, but to the subset $C_{1,2,6,7}$ by C_i. Note that this system does not invoke $\overline{\boldsymbol{U}}$ or $\overline{\Theta}$ so their potentially unstable behavior is irrelevant here. In GOMS10 the model parameters were assumed to be universal constants and L was taken to be proportional to the shortest length scale of the simulation box, $L = \min(L_x, L_y, L_z)$.

Apart from the isotropic tensor δ_{ij}, the closure terms in (21) contain only the tensor $\boldsymbol{\mathcal{R}}$ and thus do not explicitly reflect anisotropies which could be induced by $\boldsymbol{\mathcal{F}}$, or by preferred directions present already in the setup like $\boldsymbol{\Omega}$ and $\boldsymbol{g}$. The same holds *mutatis mutandis* for the closure terms in (22). A complete formulation would need to be built up from quite a number of tensorial building blocks, each accompanied with a coefficient. Possible terms up to second order in the unit vectors $\hat{\boldsymbol{\Omega}} = \boldsymbol{\Omega}/\Omega$, $\hat{\boldsymbol{g}} = \boldsymbol{g}/g$, obeying the constraint that no other pseudo–scalar than $\cos\vartheta = \hat{\boldsymbol{g}}\cdot\hat{\boldsymbol{\Omega}}$ is available, further without cross–influences of mean quantities, i.e., without using $\boldsymbol{\mathcal{F}}$ in the closure for $\boldsymbol{\mathcal{R}}$ and vice versa, are the following for $\dot{\mathcal{R}}_{ij}$:

$$\begin{aligned} &\hat{g}_i\hat{g}_j,\ \hat{\Omega}_i\hat{\Omega}_j && \text{with coefficients} \ \sim \mathcal{R}^{3/2}/L \\ &(\mathcal{R}_{il}\hat{g}_j + \mathcal{R}_{jl}\hat{g}_i)\hat{g}_l,\ (\mathcal{R}_{il}\hat{\Omega}_j + \mathcal{R}_{jl}\hat{\Omega}_i)\hat{\Omega}_l, && \quad (24) \\ &(\mathcal{R}_{il}\varepsilon_{lkj} + \mathcal{R}_{jl}\varepsilon_{lki})\hat{\Omega}_k && \text{with coefficients} \ \sim \mathcal{R}^{1/2}/L \end{aligned}$$

and for $\dot{\mathcal{F}}_i$:

$$\begin{aligned} &\hat{g}_i,\ \varepsilon_{ikl}\hat{g}_k\hat{\Omega}_l && \text{with coefficients} \ \sim \mathcal{R}^{1/2}\mathcal{F}/L \\ &\hat{g}_j\mathcal{F}_j\hat{g}_i,\ \hat{\Omega}_j\mathcal{F}_j\hat{\Omega}_i, && \quad (25) \\ &\varepsilon_{ijk}\hat{\Omega}_j\mathcal{F}_k && \text{with coefficients} \ \sim \mathcal{R}^{1/2}/L\,. \end{aligned}$$

At the pole (where $\boldsymbol{\Omega} \parallel \boldsymbol{g}$) a stationary solution of (21)–(23) is given in (B5)–(B8) where only the four quantites $\mathcal{R}_{xx} = \mathcal{R}_{yy}$, $\mathcal{R}_{zz}$, $\mathcal{F}_z$ and $\mathcal{Q}$ are different from zero. This solution agrees qualitatively with corresponding DNS results (see Sec. 3.1). Note that a closure, *extended* by the terms listed in (24) and (25), would still allow for such a solution. Several of the these terms vanish at the pole and for all the remaining ones there are structurally identical terms within the original closure. Consequently, the coefficients of these additional terms, can all be absorbed in the C_i.

Already in GOMS10, the original closure (21)–(23) was found to miss the reduction of the convective heat flux at the pole in the presence of rotation. This is an inevitable consequence of the assumption of universality (and thus $\mathbf{\Omega}$ independence) of the closure parameters, as at this location rotation is not showing up explicitly in the closure equations. Hence some modification of the model is clearly necessary. In Miller & Garaud (2007) a corresponding attempt was undertaken by assuming the length scale L of the model to be dependent on the wavelength of the most unstable convective eigenmode λ, which in turn depends on the rotation rate, thus making L also a function of the rotation rate, or $L = L(\mathrm{Ta})$. Since all model coefficients C_* appear in ratios C_*/L, a Ta dependence in L can always be transferred to the C_*. In Miller & Garaud (2007) only one of the possibilities for $L(\mathrm{Ta})$ was considered, namely a mean of λ and the distance d to the closest boundary, $L = \left(1/d^2 + 2/\lambda^2\right)$.

In this paper we adopt the view that all closure parameters must in general depend on all control parameters of the setup, namely Ta, ϑ, Ra and Pr. This is a natural lesson from mean field theory where coefficients, parameterizing the turbulence, say, in the Reynolds stress, are obtained from (approximate) solutions for the fluctuating parts of the system quantities, that is in our context, $\boldsymbol{u}$ and θ. Their governing equations contain the control parameters as coefficients, hence the fluctuating parts are in general dependent on them and thus also the mean–field coefficients (e.g. Krause & Rädler 1980; Moffatt 1978; Rüdiger 1989). As there is hardly a fundamental difference between mean–field coefficients and closure parameters, the latter can neither be universal constants.

As a first step we retain the original structure of the closure (21)–(23), but allow its coefficients C_* to vary with the control parameters, calling this model "minimally extended GOMS10 closure". We will in particular attempt to systematically identify the Taylor number and latitude dependence of the C_* and, to a lesser extent, also their dependence on Ra. Amongst the ways of extending the original GOMS10 closure to the rotating case, this seems to be the most straightforward one and rather easy to study, being also less restrictive than the approach of Miller & Garaud (2007).

Both the onset of convection and its saturated stage as functions of the rotation rate were studied by these authors, but they did not directly relate quantities like $\boldsymbol{\mathcal{R}}$ from DNS to the corresponding ones from the closure model. Our approach is here, in contrast, to derive the supposed control parameter dependences of the closure parameters referring directly to DNS results.

2.2 DNS setups

For the DNS a local Cartesian volume of size $L_x \times L_y \times L_z$ is used with $L_x = L_y$ and aspect ratio $\Gamma = L_z/L_x = 1$ or 4 with fully periodic boundary conditions and a uniform background temperature gradient as described in Sec. 2.1.

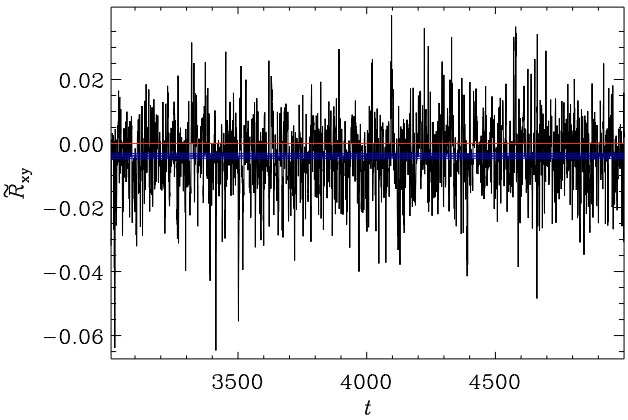

Fig. 1: Time series of $\mathcal{R}_{xy}$ from Run B4. The blue solid lines show the average and the error estimates whereas the red solid line denotes the zero level.

Grid sizes ranging from 64^3 to 512^3 are used, where the latter correspond to runs with the highest Rayleigh numbers.

The numerical simulations were performed with the PENCIL CODE[1], which uses sixth–order accurate finite differences in space, and a third–order accurate time–stepping scheme, see Brandenburg (2003); Brandenburg & Dobler (2002). Originally designed for (weakly) compressible hydrodynamics, it has recently been supplemented by a module implementing the Boussinesq approximation, following a method presented in Bell & Marcus (1992). In all cases the time integration was advanced until a statistically stationary state was reached. Typically this means that at least a few hundred convective turnover times were covered. In addition to the volume averages, time averages over this state are taken because the spatial averages still show strong temporal fluctuations. Errors are estimated by dividing the time series into three equally long parts and computing mean values for each part individually. The largest departure from the mean value computed for the whole time series is taken to represent the error. A typical example is shown in Figure 1.

3 Results

3.1 DNS Runs

The DNS runs are summarised in Table 1, for more details see Table C1 in Appendix C. Each of the Sets A–G is designated to investigate a certain fixed latitude between the pole and the equator while the rotation rate is varied. Z denotes the non–rotating run. The ranges for the Reynolds, Rayleigh, and Coriolis numbers as well as U_{rms} probed by the DNS are also listed.

In the DNS runs we had to deal with a numerical stability problem in the transition from the kinematic, exponentially growing, stage to the non–linear saturated state if the Rayleigh number was too small. Since this instability was

[1] http://pencil-code.googlecode.com/

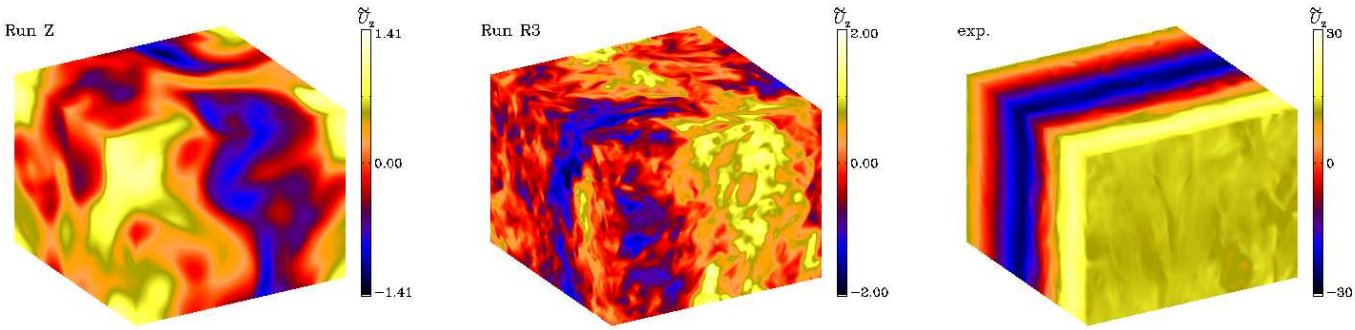

Fig. 2: Velocity component U_z in units of $d(\alpha g G_0)^{1/2}$ from non–rotating DNS runs Z (left) and R3 (center) with $\mathrm{Ra} = 3 \cdot 10^5$ and $\mathrm{Ra} = 2.5 \cdot 10^7$, respectively. The rightmost panel is from an experimental run with a very high rotation rate ($\mathrm{Ta} = 10^{10}$) and $\mathrm{Ra} = 3 \cdot 10^5$ at $\vartheta = 75^\circ$.

suppressed by rotation, it was possible to circumvent this problem by starting runs with high values of Ta ($\approx 10^7$) which allowed a statistically stationary state to be established. Then we gradually lowered Ta until the desired parameter range had been reached. Eventually we were able to successfully perform non–rotating runs in the low Rayleigh number regimes using this method. A snapshot of the vertical velocity in this Run Z is pictured in Fig. 2. When the Rayleigh numbers were increased, this numerical instability became manageable. In the time series of the statistically stationary state, we observe large fluctuations and intermittent exponential growth. These features are most likely manifestations of the so–called "elevator modes", described in Calzavarini et al. (2006). The numerical instability at low Rayleigh numbers may be related to these modes: If the mode grows too rapidly, the code might not be able to handle it. They are exponentially growing solutions of the *nonlinear* Boussinesq system (9), (11). Secondary instabilities limit their growth ultimately, but for a box with an aspect ratio of unity this is known to happen only at high mode amplitudes. In our setup, the elevator modes exist uninfluenced by rotation at any latitude in the form $[0, 0, U_z(y)] \sim \exp(\lambda + \mathrm{i}k_y y)$ and are exponentially growing if $\mathrm{Ra} > (dk_y)^4$. At the pole an additional dependence on x is possible. When admitting a horizontal velocity component, another type of exponentially growing solutions of the nonlinear equations is possible at the equator, having the form $[0, U_y(x), U_z(x)] \sim \exp(\lambda t + \mathrm{i}k_x x)$. The critical Rayleigh number is then given by $(dk_x)^4 + \mathrm{Ta}$. In any case such growing modes should be affected by rotation, insofar as the secondary instabilities will also certainly be modified by the Coriolis force.

The geometry of the elevator modes as seen in a rapidly rotating run ($\mathrm{Ta} = 10^{10}$) at $\vartheta = 75^\circ$ is demonstrated in the rightmost panel of Fig. 2. The depicted large–scale flow pattern ("stripe") appears and disappears repeatedly in our simulations, coinciding with the large fluctuations mentioned above. This pattern manifests itself ever more clearly when the rotation rate is increased: At the lowest rates, it is only seen blurred by the usual small–scale fluctuations, while for intermediate rates its periodical appearance and reconfiguration blots the time–series with periods of exponential growth and decay. At very high rotation rates the stripe feature becomes permanent, with very high values of velocity and temperature. This is why some runs in the rapid rotation regime needed to be omitted, namely when the flow pattern was completely dominated by the elevator mode and no turbulence was present. The trouble caused by these modes intensifies as colatitude increases, as they start to dominate the flow dynamics at lower Taylor numbers.

The DNS were further complicated by convergence issues. Increasing only the spatial resolution had only a minor effect in the results even at the largest values of Ta. However, reducing the time step δt affected the results more dramatically requiring many of the simulations to run for far longer than initially expected. This problem became more pronounced in the rapid rotation regime. We obtained converged results by reducing the time step by a factor of two to three until the results from the two shortest δt agreed within 20 per cent. In singular cases this issue led to excluding runs completely, if reasonably long timesteps could not be used.

3.2 Calibration of the closure model

In this section we assume at first that the diffusive coefficients $C_{\nu,\nu\chi,\chi}$ vanish. However, they can be thought to be subsumed in the coefficients $C_{1,6,7}$, see Eq. (32), and we will make an effort to disentangle them in Sec. 3.2.5 in the context of Rayleigh number dependence.

Stationary solutions of the closure model Eqs. (B1) result for given C_i from the corresponding nonlinear *algebraic* system of equations. This opens up systematic ways of calibrating the parameters and of studying thereby the performance of the "minimally extended GOMS10" model. Two such methods are described here.

The DNS results are qualitatively compatible with the specific solution (B5)–(B8) at the pole for all rotation rates

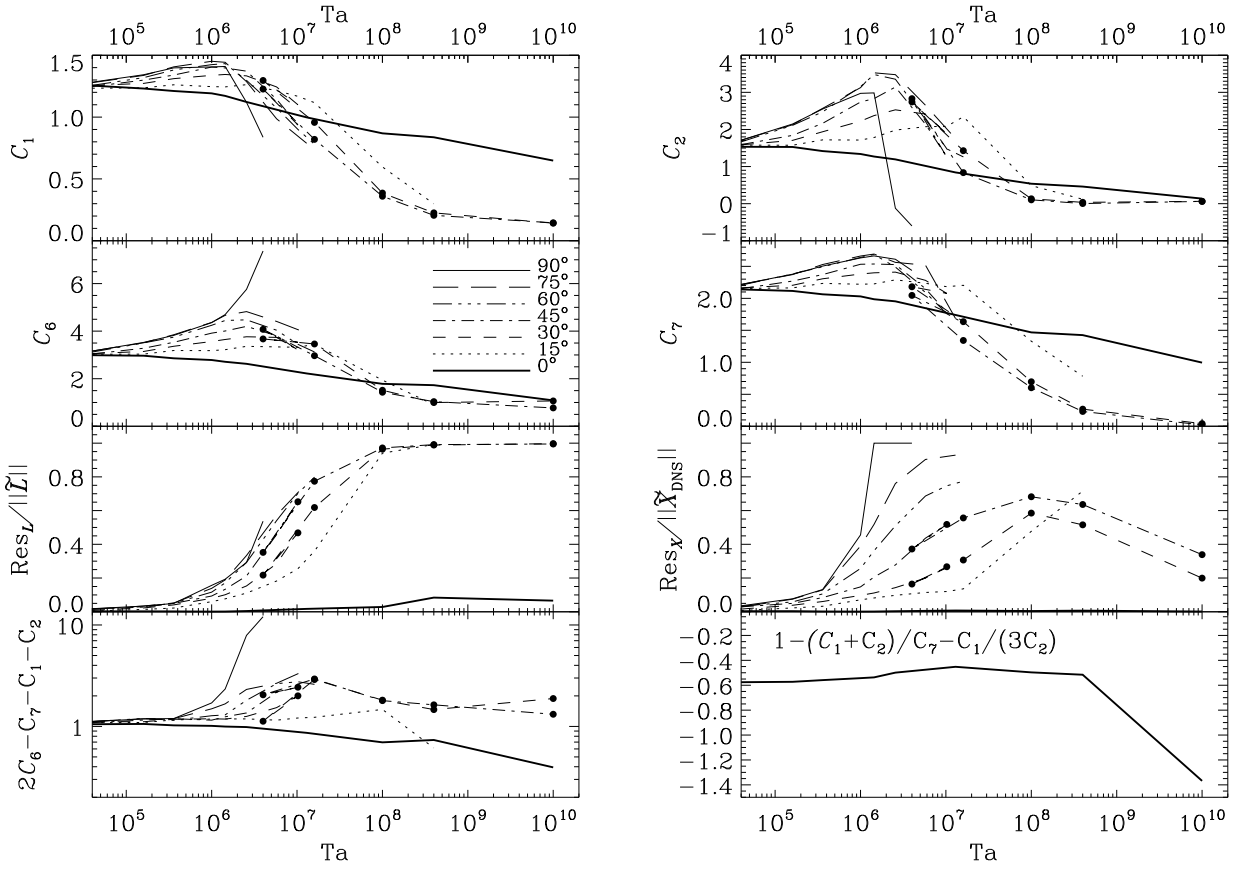

Fig. 3: Closure parameters from the least–squares approach for Sets A–G and Z ($\mathrm{Ra} = 3 \cdot 10^5$, $\mathrm{Pr} = 0.6$). Upper four panels: C_i as functions of Ta; Third row: normalized residuals (27) and (28). Bottom row: left–hand sides of constraint (29) and stability constraint (30) (for $\vartheta = 0$ only). Symbols: data points for DNS with viscous heating included, see Sec. 2.1.1

considered, insofar to good accuracy $\mathcal{R}_{xy,xz,yz}, \mathcal{F}_{x,y} = 0$, see Table C1 in Appendix C.

3.2.1 Least–squares fit

One can ask, whether any set of closure parameters C_i can be found so that the stationary results from the closure model reproduce exactly the results from a statistically stationary stage of a corresponding DNS run. A straightforward way to check this is to insert the parameters (αg, Ω_0, G_0) used in the DNS together with their (temporally averaged) results for $\boldsymbol{\mathcal{R}}$, $\boldsymbol{\mathcal{F}}$ and $\mathcal{Q}$ into the time–independent version of the system (B1). Treating the C_i as unknown variables, a generally overdetermined system of linear equations for them (ten equations vs. four variables) of the form

$$\boldsymbol{N}\boldsymbol{c} = \boldsymbol{L} \tag{26}$$

is obtained where $\boldsymbol{c} = [C_1, C_2, C_6, C_7]$. The matrix $\boldsymbol{N}$ is derived from the closure terms and the vector $\boldsymbol{L}$ contains all remaining ones, such as the Coriolis and buoyancy terms, see Eqs. (B1). Because of the overdetermination one can in general not expect to find any set of coefficients C_i with which the closure reproduces all the modeled quantities perfectly. At the pole, however, there are only four linearly independent equations in the system (26), making it unambiguously solvable. The solution is given explicitly in Appendix B. At all other latitudes this system can be solved only approximately using the standard linear least–squares method, that is, solving the regular system $\boldsymbol{N}^{\mathrm{T}}\boldsymbol{N}\boldsymbol{c} = \boldsymbol{N}^{\mathrm{T}}\boldsymbol{L}$, where the superscript "T" denotes transposition. The results for $\boldsymbol{c}$ are shown in Fig. 3 as functions of Taylor number and colatitude. As a test of the consistency of the Eq. (26) we calculated the residual norm

$$\mathrm{Res}_{\boldsymbol{L}} = ||\widetilde{\boldsymbol{N}\boldsymbol{c}_{\mathrm{ls}}} - \widetilde{\boldsymbol{L}}||, \tag{27}$$

where the subscript "ls" refers to the least–squares solution, tildes denote normalizations and $||\cdot||$ denotes the Euclidian norm, see Fig. 3. The normalization of the vectors $\boldsymbol{N}\boldsymbol{c}_{\mathrm{ls}}$ and $\boldsymbol{L}$ is necessary because of the differing dimensions of their components. The components originating from the Reynolds stresses equation are normalized by $(\alpha g G_0)^{3/2} d^2$, those from the heat fluxes by $\alpha g (G_0 d)^2$, and those from the temperature variance by $(\alpha g G_0^5)^{1/2} d^2$. The quality of the obtained solution can also be measured by calculating the difference in the stationary solutions for $\boldsymbol{X} = (\mathcal{R}_{xx}, \ldots, \mathcal{R}_{zz}, \mathcal{F}_x, \mathcal{F}_y, \mathcal{F}_z, \mathcal{Q})$ from the closure model (B1) with $\boldsymbol{c} = \boldsymbol{c}_{\mathrm{ls}}$ and from the corresponding tempo-

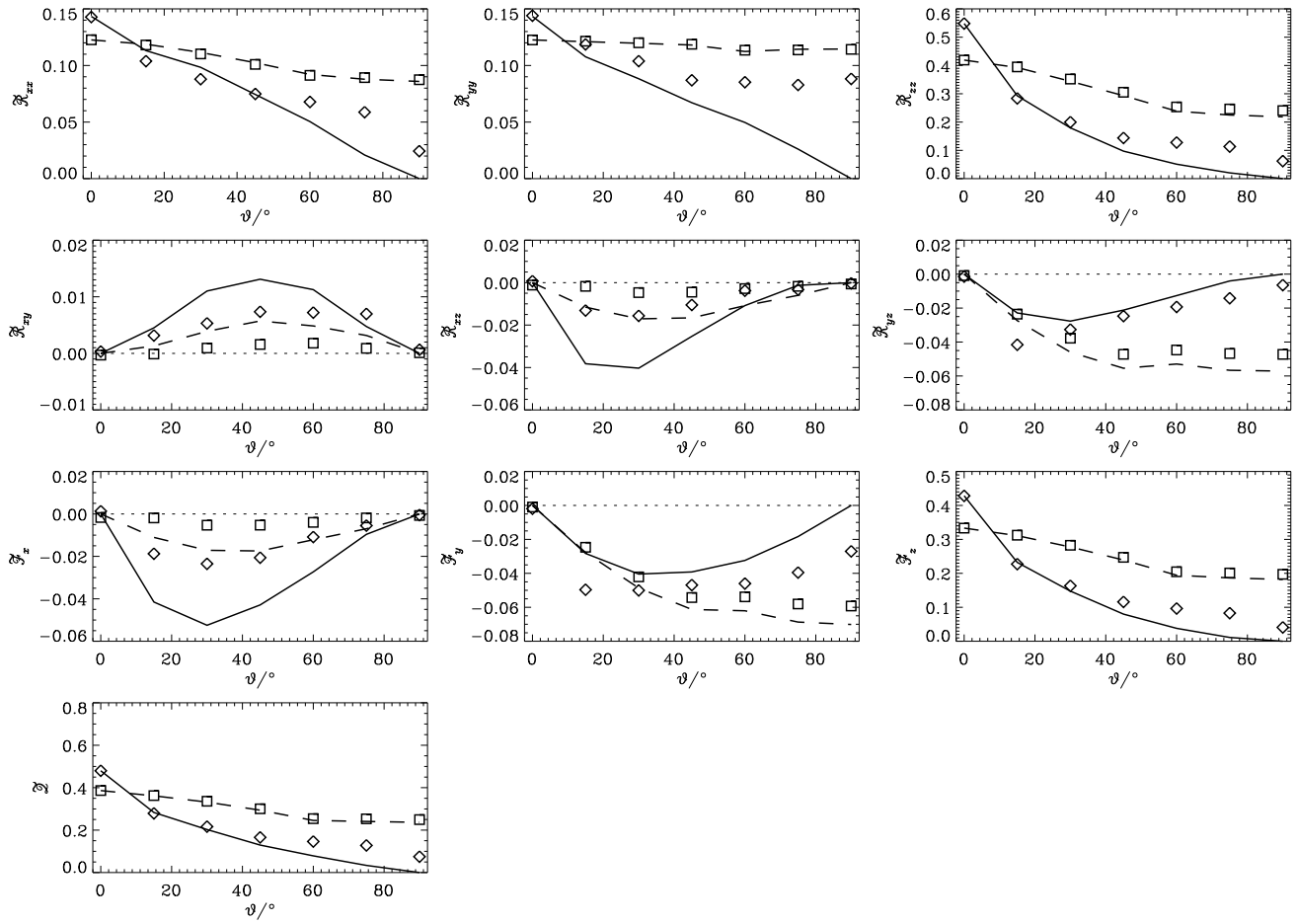

Fig. 4: Results of the closure model (lines) for the quantities $\boldsymbol{\mathcal{R}}$, $\boldsymbol{\mathcal{F}}$ and $\mathcal{Q}$ with coefficients C_i from the least–squares fit compared with the corresponding DNS results (symbols) both as functions of colatitude ϑ. Reynolds stress, heat flux, and temperature variance are normalized by U_0^2, $d\,U_0 G_0$ and $(d\,G_0)^2$, respectively, with $U_0 = d(\alpha g G_0)^{1/2}$ (indicated by tildes). Dashed lines/squares: slow rotation (Runs A2–G2 with $\mathrm{Ta} = 1.6 \cdot 10^5$), solid lines/diamonds: faster rotation (Runs A6–G6 with $\mathrm{Ta} = 2.56 \cdot 10^6$). Note that the C_i depend on Ta and ϑ, see Fig. 3. Error bars associated with the DNS runs are not plotted since they are at most as large as the symbols.

rally averaged results of the DNS run, that is, by calculating the residual

$$\mathrm{Res}_{\boldsymbol{X}} = ||\widetilde{\boldsymbol{X}}_{\mathrm{closure}} - \widetilde{\boldsymbol{X}}_{\mathrm{DNS}}||, \tag{28}$$

where tildes refer to normalization: by $\alpha g G_0 d^2$ for $\boldsymbol{\mathcal{R}}$, by $G_0^{3/2}(\alpha g)^{1/2} d^2$ for $\boldsymbol{\mathcal{F}}$, and by $(G_0 d)^2$ for $\mathcal{Q}$. The residual (28) is also shown in Fig. 3 together with the left hand sides of the realizability condition

$$2C_6 - C_7 - C_1 - C_2 \geq 0 \tag{29}$$

given in GOMS10 and the stability condition

$$1 - \frac{C_1 + C_2}{C_7} - \frac{C_2}{3C_1} < 0 \tag{30}$$

for the pole as derived in Appendix B. The solutions $\boldsymbol{X}_{\mathrm{closure}}$ and $\boldsymbol{X}_{\mathrm{DNS}}$ are directly compared in Fig. 4.

From Fig. 3 one can see that the derived model coefficients change with colatitude and Taylor number, with following patterns: at the pole they fall with growing Ta, but not so for any other colatitude. Instead, with the exception of C_6 at the equator, they first grow with Ta and then start falling at $\mathrm{Ta} \approx 10^6 \ldots 2 \cdot 10^7$ depending on colatitude. Both the growth and the fall become steeper with growing colatitude. For each C_i, the curves for different ϑ converge as Ta approaches zero as expected. Although the least–squares method has no built–in way of adhering to the conditions (29) and (30), we see that these are fulfilled nevertheless.

Using the (exact) results for the non–rotating run Z we computed the ratios of the coefficients C_i and compared them to the corresponding ratios from GOMS10, and Snellman et al. (2012a,b), hereafter S12a and S12b, in Table 2. Also listed in the table are the ratios resulting from the non–rotating higher Rayleigh number runs that will be discussed in Sec. 3.2.5. These ratios are important because any difference in the results for C_i in the non–rotating case could be due to a badly chosen length scale L, which is canceled by the ratios. Except for C_2/C_6, we see that our values are at

Table 1: Summary of the DNS runs at different colatitudes ϑ. $\mathrm{Pr} = 1$ for sets R and R', and $\mathrm{Pr} = 0.6$ for all other sets. $\mathrm{Ta} = 4 \cdot 10^4 \ldots \cdot 10^{10}$ for sets A through G, $\mathrm{Ta} = 0$ for sets Z and R, and $\mathrm{Ta} = 10^6$ for R'.

Set	ϑ	$\mathrm{Ra}[10^5]$	Re	Co	$U_{\mathrm{rms}}/d\sqrt{\alpha g G_0}$
Z	–	3	87	0	0.77
A	0°	3	$91-235$	$0.06-10.79$	$0.81-2.09$
B	15°	3	$80-296$	$0.06-1.73$	$0.71-2.63$
C	30°	3	$70-798$	$0.06-3.18$	$0.64-7.09$
D	45°	3	$62-1143$	$0.06-2.22$	$0.55-10.16$
E	60°	3	$58-101$	$0.06-1.01$	$0.51-0.89$
F	75°	3	$54-86$	$0.06-1.06$	$0.48-0.77$
G	90°	3	$47-85$	$0.06-1.08$	$0.42-0.76$
R	–	$2.5-2000$	$68-2358$	0	$0.80-1.04$
R'	0°	$10-250$	$128-764$	$0.03-0.2$	$0.81-0.96$

Table 2: Ratios of the coefficients C_i obtained by the least–squares approach from the non–rotating runs with different Rayleigh numbers compared to GOMS10 and S12a,b.

Run	$\mathrm{Ra}\,[10^6]$	C_1/C_2	C_1/C_6	C_1/C_7	C_2/C_6	C_2/C_7	C_6/C_7
Z	0.30	0.81	0.42	0.58	0.51	0.72	1.40
R1	0.25	0.92	0.45	0.68	0.49	0.73	1.50
R2	1	0.73	0.39	0.64	0.53	0.87	1.65
R3	4	0.68	0.35	0.59	0.51	0.87	1.69
R4	10	0.80	0.36	0.58	0.46	0.73	1.60
R5	25	0.83	0.36	0.57	0.44	0.68	1.56
R6	200	0.90	0.37	0.55	0.41	0.60	1.47
GOMS10	50	0.66	0.29	0.29	0.43	0.43	1.00
S12a	–	≈ 0.4	–	–	–	–	–
S12b	–	–	–	–	–	–	≈ 2.1

odds with those of GOMS10 and S12a,b. In the latter cases this is not surprising since S12a,b deal with forced turbulence and passive scalar transport, respectively.

As for the residuals, they unsurprisingly vanish (as long as $\mathrm{Ta} \lesssim 2 \cdot 10^6$) at the pole, otherwise rise with Taylor number while the colatitude has only a small effect on the residual (27), but a stronger one on (28), see Fig, 3, 3rd row. The reason why the residuals do not vanish as expected at the pole for high Taylor numbers turns out to lie in small deviations of the DNS data from what is theoretically predicted: the off–diagonal Reynolds stresses $\mathcal{R}_{xy,xz,yz}$ and the heat fluxes $\mathcal{F}_{x,y}$ are not exactly zero. This is due to the fact that very long time integrations are needed for the time–averaged quantities to converge for high fluctuation levels. The effect of these discrepancies, however, is minor when compared to the effect of diverging $\mathcal{R}_{xx}$ and $\mathcal{R}_{yy}$, which should, on grounds of symmetry, be equal at the pole. But as can be seen in Table C1, the DNS results for them are somewhat different at high rotation rates, again because of incomplete temporal convergence. The least–squares method can only produce a perfect match with the DNS if the number of linearly independent closure equations equals the number of model parameters, and both of the aforementioned deviations disturb this equivalence.

Another quirk exhibited by the different residuals is that they do not fully correlate with each other: while $\mathrm{Res}_{\boldsymbol{L}}/||\widetilde{\boldsymbol{L}}||$ seems to tend to unity at all colatitudes except for the pole, $\mathrm{Res}_{\boldsymbol{X}}/||\widetilde{\boldsymbol{X}}_{\mathrm{DNS}}||$ does not behave the same way, and in some cases ($\vartheta = 30°, 45°$) it even decreases with increasing rotation. The reason for these differences is that the residuals measure completely different things. The former measures the quality of the least–squares solution of 26 and the latter shows the difference of the closure, employing the fitted coefficients, and the DNS results.

At the equator the normalized residual $\mathrm{Res}_{\boldsymbol{X}}/||\widetilde{\boldsymbol{X}}_{\mathrm{DNS}}||$ settles at unity for $\mathrm{Ta} \gtrsim 1.44 \cdot 10^6$. This is because the analytical results from the closure become very small for all the modeled quantities indicating that the obtained C_i do not allow for any other than the trivial solution of (B1). Setting a reasonable threshold for $\mathrm{Res}_{\boldsymbol{X}}/||\widetilde{\boldsymbol{X}}_{\mathrm{DNS}}||$, one can derive for the least–squares results applicability margins as functions of Ta and ϑ.

The DNS results $\boldsymbol{X}_{\mathrm{DNS}}$ for a slow and a rapid rotation case are compared with the corresponding closure results obtained with the derived model coefficients in Fig. 4. At slow rotation the DNS and the closure results are visibly closer to each other than at rapid rotation. Further, the fit for small quantities like $\mathcal{R}_{xy,xz,yz}$ or $\mathcal{F}_{x,y}$ is significantly worse than for the larger ones, like $\mathcal{R}_{zz}$, $\mathcal{F}_z$ or $\mathcal{Q}$.

3.2.2 Optimization approach

The least–squares approach shows that the stationary closure model cannot perfectly match the DNS with any set of model coefficients outside the pole, and this failure becomes progressively worse as the rotation rate is increased. As a method of calculating the C_i, this approach is inflexible: the matrix $\boldsymbol{N}$ and vector $\boldsymbol{L}$ are determined by the DNS-results inserted into (B1), and the method minimizes $\mathrm{Res}_{\boldsymbol{L}}$ rather than $\mathrm{Res}_{\boldsymbol{X}}$. In order to determine the model coefficients while improving the agreement between the closure and the DNS results, we formulate the following optimization problem: minimize the *objective function*

$$(\widetilde{\boldsymbol{X}}_{\mathrm{closure}} - \widetilde{\boldsymbol{X}}_{\mathrm{DNS}})^2 = \mathrm{Res}^2_{\boldsymbol{X}} \tag{31}$$

obeying the constraints $C_i > 0$ and (29). The problem was tackled by the Generalized Reduced Gradient Method (Lasdon et al. 1978) as implemented by the IDL routine CONSTRAINED_MIN with the nonlinear system from Eqs. (B1) being solved by Newton iteration (IDL routine NEWTON).

The optimum results are shown in Fig. 5 where the upper four panels refer to the C_i while the lower left panel gives the residual (28) and the lower right one shows the value of the quantity $2C_6 - C_7 - C_1 - C_2$ from the constraint (29). Along with the dependence of the coefficients on Ta, there is again in general a separate one on ϑ. At the pole ($\vartheta = 0$) $\mathrm{Res}_{\boldsymbol{X}}$ assumes exceptionally low values (not shown). This is a consequence of the already mentioned degeneration which allows to determine the C_i uniquely from the $\boldsymbol{X}_{\mathrm{DNS}}$. Hence the residual should actually vanish and its observed values are essentially due to the imperfectness of the stationary DNS solution as discussed above. Apart from the pole, the quality of the optimum is in general decreasing with growing Ta, yet having only a weak dependence on colatitude. It can be considered good (say, up to 20% in $\mathrm{Res}_{\boldsymbol{X}}/||\widetilde{\boldsymbol{X}}_{\mathrm{DNS}}||$) when $\mathrm{Ta} \lesssim 3 \cdot 10^7$ at $\vartheta = 15°$, or when $\mathrm{Ta} \lesssim$ a few10^6 at other latitudes. Also for $\vartheta = 30°, 45°$ and $\mathrm{Ta} \gtrsim$ a few 10^9 the accuracy improves to aforementioned levels. For $\vartheta = 45°, 60°$ and $1.44 \cdot 10^6 < \mathrm{Ta} < 4 \cdot 10^8$ the constraint (29) becomes active in the sense that the optimum lies then on the margin of the admissible domain, that is, $2C_6 - C_1 - C_2 - C_7 = 0$ (red curve sections in Fig. 5). C_1 and C_7, apart from initially displaying very sligthly growing tendencies (for $\mathrm{Ta} \lesssim 2 \cdot 10^6$ and $4 \cdot 10^6$, respectively), show in general a monotonously falling dependence on Ta. The dependences resemble Lorentzians (for C_1 at least when $\mathrm{Ta} < 10^8$). In contrast, C_2 and C_6 are falling monotonously with Ta only at the pole. At larger ϑ the Ta dependencies of C_2 show maxima in the interval $4 \cdot 10^5 < \mathrm{Ta} < 3 \cdot 10^7$, while for C_6 maxima are detected only for $15° < \vartheta < 60°$. In all, the behavior of the latter two coefficients seems less systematic than that of C_1 and C_7.

By comparing the residuals $\mathrm{Res}_{\boldsymbol{X}}/\widetilde{\boldsymbol{X}}_{\mathrm{DNS}}$ in Figs. 5) and 3 one sees that for larger Taylor numbers it remains clearly lower for the optimization approach ($\lesssim$ 50% vs. up to 100 %). This means that this approach succeeds in finding closure parameters with better matching results for $\boldsymbol{X}$, as intended. When comparing the results of the two approaches for the C_i we find fair qualitative agreement in the patterns of change of C_i, with few exceptions, although there are noticeable quantitative differences in values.

Given that, apart from the constraint (29), also the stability properties of the closure model should not differ from that of the DNS, we enhanced the optimization problem by the constraint that for the optimum fit the stationary solution corresponding to it should be stable. For that, we linearized the system (B1) about the state $\boldsymbol{X}_{\mathrm{closure}}$, obtaining a system of the form $\partial_t(\boldsymbol{\delta X}) = \boldsymbol{A} \cdot \boldsymbol{\delta X}$ for the perturbations $\boldsymbol{\delta X}$, and required that the maximum of the real parts of the eigenvalues of $\boldsymbol{A}$ is negative. To avoid influences of numerical noise we set their upper bound to a small negative value instead of zero. The matrix eigenvalue problem was solved by means of the IDL routines LA_ELMHES and LA_HQR. It turned out that the additional constraint is never active, that is, stability is already granted if (29) is obeyed.

Table 3: Ratios of the coefficients C_i obtained for rotating runs by the optimization approach without (upper block) and with (lower block) viscous heating included. The minimal Ta is $4 \cdot 10^4$ and $4 \cdot 10^6$, respectively.

ϑ [°]	max(Ta)	C_1/C_2	C_1/C_6	C_1/C_7
0	10^{10}	$0.81 - 4.74$	$0.42 - 0.60$	$0.57 - 0.65$
15	$4 \cdot 10^8$	$0.38 - 0.78$	$0.24 - 0.41$	$0.38 - 0.57$
30	10^7	$0.27 - 0.79$	$0.27 - 0.41$	$0.54 - 0.58$
45	10^7	$0.10 - 0.77$	$0.15 - 0.41$	$0.54 - 0.58$
60	$1.6 \cdot 10^7$	$0.03 - 0.74$	$0.05 - 0.40$	$0.50 - 0.57$
75	$1.3 \cdot 10^7$	$0.02 - 0.73$	$0.03 - 0.40$	$0.41 - 0.58$
90	$4 \cdot 10^6$	$0.28 - 2.38$	$0.08 - 0.40$	$0.35 - 0.58$
30	10^{10}	$0.23 - 0.64$	$0.13 - 0.32$	$0.56 - 3.46$
45	10^{10}	$0.06 - 0.21$	$0.11 - 0.21$	$0.60 - 6.93$

In Fig. 6 the DNS and closure model results as functions of the colatitude are given for the same two Taylor numbers as in Fig. 4. Obviously, amongst the dominant variables, $\mathcal{R}_{zz}$, $\mathcal{F}_z$, and $\mathcal{Q}$ are very well fitted. For slow rotation, also $\mathcal{R}_{xx}$, $\mathcal{R}_{yy}$, show good fits, and $\mathcal{R}_{yz}$, $\mathcal{F}_y$ yet acceptable fits. At the higher rotation rate $\mathcal{R}_{xx}$, $\mathcal{R}_{yy}$, $\mathcal{R}_{yz}$, and $\mathcal{F}_y$ are also acceptable. In all, we have to conclude that the incompleteness of the closure ansatz is most relevant in the quantities $\mathcal{R}_{xy,xz}$ and $\mathcal{F}_x$ while there is apparently nothing important missing in the ansatzes for $\mathcal{R}_{zz}$ and $\mathcal{Q}$. Thus, a guideline can be given how to enhance the ansatzes with the added terms having maximum effect: for $\mathcal{R}_{xz,yz}$ and $\mathcal{F}_x$ these could be terms of the form $\hat{\Omega}_i\hat{\Omega}_j$, $(\mathcal{R}_{il}\hat{\Omega}_j + \mathcal{R}_{jl}\hat{\Omega}_i)\hat{\Omega}_l$ or $(\mathcal{R}_{il}\varepsilon_{lkj} + \mathcal{R}_{jl}\varepsilon_{lki})\hat{\Omega}_k$ and $\varepsilon_{ikl}\hat{g}_k\hat{\Omega}_l$, $\hat{\Omega}_j\mathcal{F}_j\hat{\Omega}_i$ or $\varepsilon_{ijk}\hat{\Omega}_j\mathcal{F}_k$, respectively, see Sec. 2.1.3.

Again, the ratios C_1/C_2 and C_6/C_7 for the non–rotating case are at odds with GOMS10, see Table 3.

3.2.3 Dependence on Ta

For both approaches, the obtained C_i show a clear dependence on Ta. As long as the fit quality is satisfactory, that is for Ta up to a few times 10^6 for which the effect of the neglect of closure terms constructed from $\boldsymbol{\Omega}$ should be small (see Sec. 2.1.3), and again for $\mathrm{Ta} \gtrsim 10^9$ these dependencies might be taken as physical, but we are faced with the ambiguity between the two fitting approaches. At the pole, however, the fit quality is perfect and no ambiguity occurs. As discussed above, the used closure ansatzes are here complete at least up to the level represented by (24), (25). Hence, the Ta dependences of the C_i are here the more trustworthy. On the one hand, the DNS results are consistent with the specific solution (B5)–(B8) for the pole, which was derived from the closure model, but on the other hand they clearly depend on Ω while there is no explicit occurrence of $\boldsymbol{\Omega}$ in the specific solution. We interpret this as a confirmation of our statement in Sec. 2.1.3 that the closure should be extended by making the coefficients Ω (or Ta) dependent.

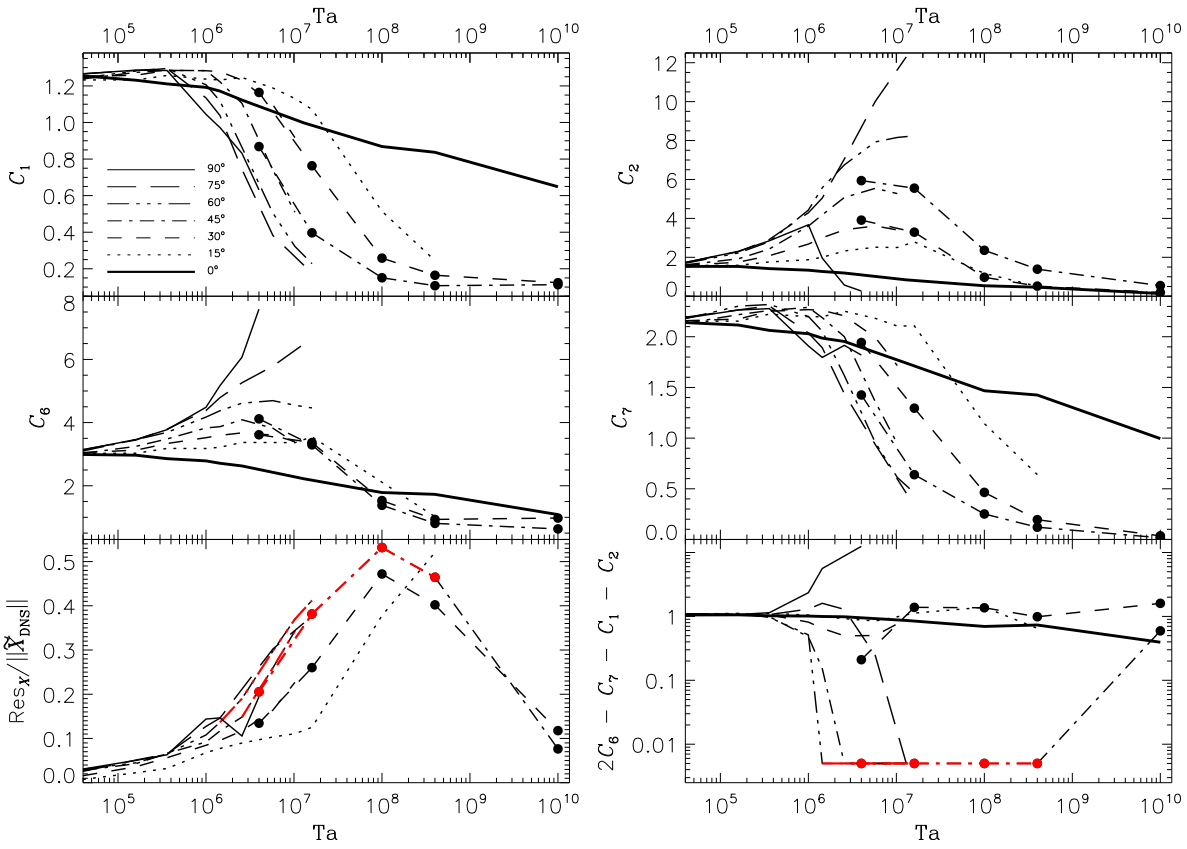

Fig. 5: Closure parameters from the optimization approach for Sets A–G ($\mathrm{Ra} = 3 \cdot 10^5$, $\mathrm{Pr} = 0.6$). Upper four panels: C_i as functions of Ta and colatitude ϑ. Lower left panel: normalized residual (28) at optimum; values for $\vartheta = 0°$ are omitted because they are very small. Lower right: value of the left–hand side of the constraint (29). For legibility (numerical) zero values were replaced by an arbitrary small constant. Red curve sections: regions where this constraint is active. Symbols: data points for DNS with viscous heating included.

Apart from the pole, the quality of the fit from the optimization approach is gradually worsening with increasing rotation rate up to $\mathrm{Ta} \approx 10^8$, but improves again beyond that letting the normalized residual adopt values $\approx 10\%$ for $\mathrm{Ta} = 10^{10}$. We take this as an indication of a most pronounced importance of closure terms constructed from $\boldsymbol{\Omega}$ for medium rotation rates $(\text{a few } 10^6) \lesssim \mathrm{Ta} \lesssim (\text{a few } 10^9)$. In this range the Ω (and ϑ) dependence induced by those terms cannot be adequately "mimicked" by corresponding dependences of the C_i. In contrast, for slow and rapid rotation the original ansatz performs satisfactorily well.

3.2.4 Dependence on the box aspect ratio

The elevator modes are known to be only weakly damped for a box of aspect ratio unity in the non–rotating case (or at the pole). Hence, in order to assess their influence particularly at other latitudes we performed a series of runs for the chosen set of latitudes with $\Gamma = L_z/L_x = L_z/L_y = 4$, $\mathrm{Ra} = 3 \cdot 10^5$ and a moderate rotation rate of $\mathrm{Ta} \approx 10^9$ or $4 \cdot 10^6$ defined with d in (16) taken as the z or horizontal extent of the computational box, respectively. The runs are listed in Table C4.

The results for the C_i, obtained by the optimization–based fit, are shown in Fig. 7 in combination with results for $\Gamma = 1$ where comparability was ensured by equating the Taylor numbers defined with the horizontal rather than the vertical extent of the box. Apart from the pole and the equator there is only a weak influence of the aspect ratio which supposedly does not exceed the general uncertainties in the determination of the C_i. When approaching the pole, there are systematically stronger deviations in C_2 and C_6 which we take as an indication of changes in the overall statistical properties of the turbulence due to the Γ dependent damping of the elevator modes. Such changes are visible in the time series of the quantities $\boldsymbol{X}$: For $\Gamma = 1$ both the temporal averages and the magnitudes of the temporal fluctuations are clearly higher than for $\Gamma = 4$. The frequency of sharp high–amplitude peaks is higher in the former case and the time series has a somewhat clearer quasiperiodic character. At the equator the coefficients deviate drastically and we suppose that there is indeed some qualitative change in the turbulence when elongating the box.

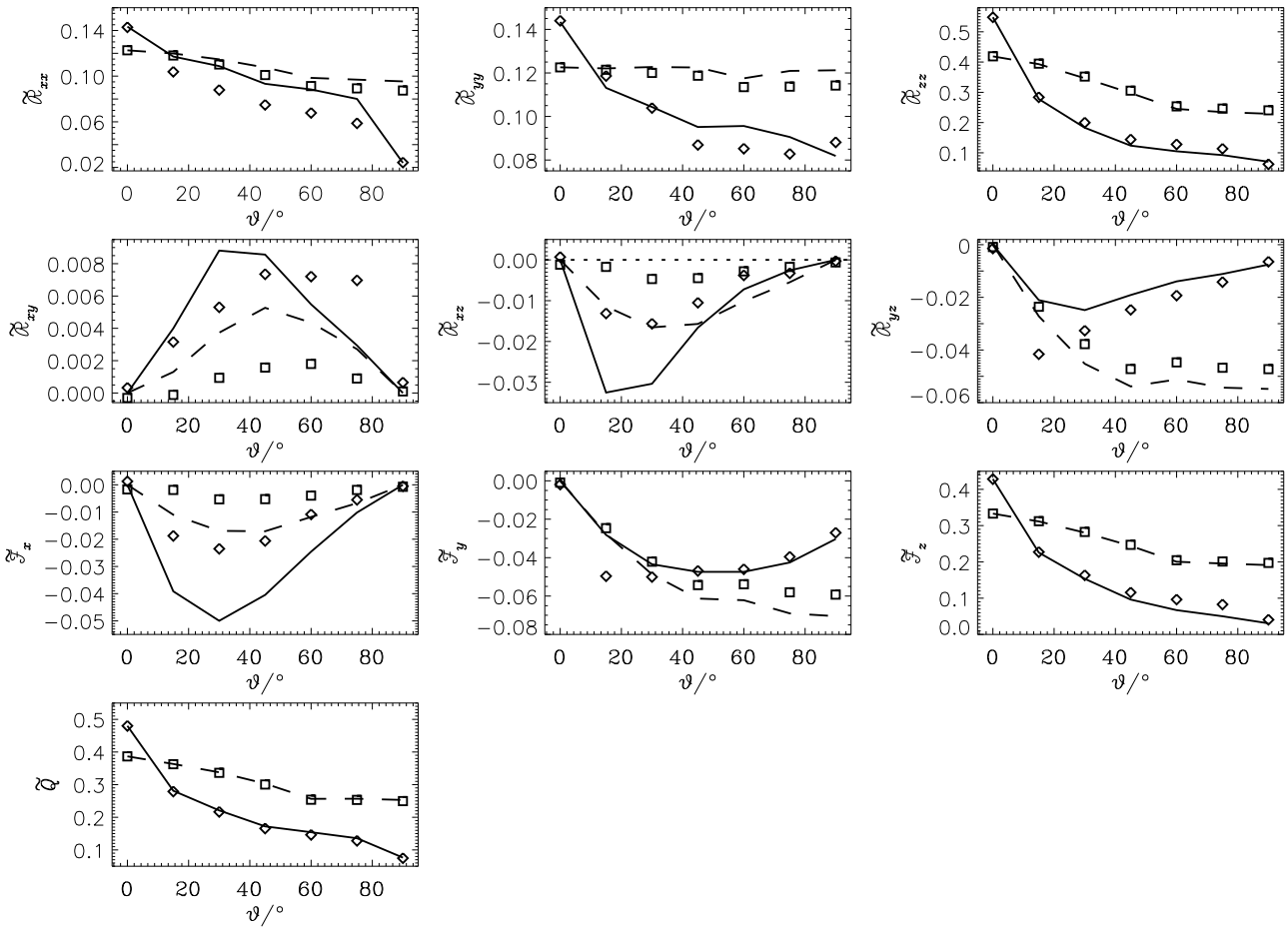

Fig. 6: Same as Fig. 4 but with the C_i from the optimization approach.

As a spot check we also performed one run with $\Gamma = 0.75$ (one of the cases considered in GOMS10) and $\vartheta = 45°$, $\mathrm{Ta} \approx 5{\cdot}10^6$. Again a stationary state was reached albeit with an even stronger quasi–periodicity in its time series compared to $\Gamma = 1$. The coefficients are very close to those obtained with $\Gamma = 1$ and 4, see the symbols in Fig. 7. We conclude that at not too small rotation rates and colatitudes the influence of the box aspect ratio on the coefficient values is not important.

3.2.5 Dependence on Ra

Due to computational constraints as a consequence of the required higher resolution, we have not studied Rayleigh numbers higher than $\mathrm{Ra} = 3 \cdot 10^5$ in detail. This is relevant because the comparison study, GOMS10, employed values up to two orders of magnitude higher. In order to see how our results are influenced by the Rayleigh number we performed two sets of runs with higher Ra and $\mathrm{Ta} = 0$ (up to $\mathrm{Ra} = 2 \cdot 10^8$) as well as $\mathrm{Ta} = 10^6$, $\vartheta = 0°$ (up to $\mathrm{Ra} = 2.5 \cdot 10^7$). Since both of these cases are exactly solvable, we use the least–squares method to calculate the model coefficients. The Rayleigh numbers were changed by adjusting the diffusivity parameters χ and ν, while keeping the Prandtl and Taylor numbers constant. The results are summarised in Table 1 and shown in Fig. 8. Table C2 in Appendix C gives more details. The resulting ratios of the coefficients C_i for the non–rotating case are also listed in Table 2.

From Fig. 8 we see that the values of the coefficients C_2 and C_6 rise somewhat with increasing Rayleigh number and then fall below their initial values, while C_1 and C_7 fall monotonously. The ratios of the coefficients shown in Table 2 exhibit different behaviors with increasing Ra, from monotonously falling (C_1/C_6 and C_1/C_7) to first falling and then rising (C_1/C_2) and first rising and then falling (all others).

The parameters obtained from the rotating runs are rather similar to those from the non–rotating runs, with the difference that also $C_{2,6}$ are monotonously decreasing with Ra. For the highest $\mathrm{Ra} = 2.5 \cdot 10^7$ the results for the non–rotating and rotating cases are very close to each other. This is because the rotational influence on the flow, measured by Co, is for constant Ta decreasing with increasing Ra. The behavior of the C_i from the rotating cases suggests convergence to some constant values at high Ra, but even higher Ra runs would be needed to verify this. In the non–rotating case a tendency towards convergence for higher values of

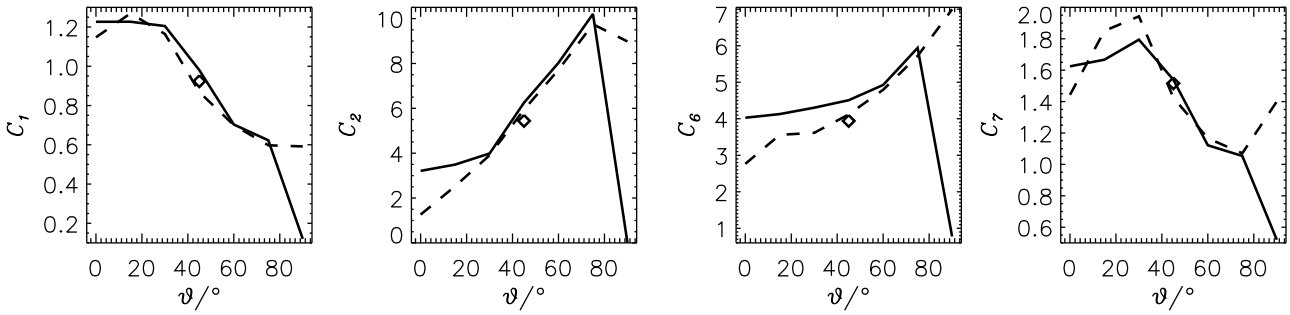

Fig. 7: Closure coefficients C_i for box aspect ratios $\Gamma = 4$ (solid) and $\Gamma = 1$ (dashed) both with $\mathrm{Ra} = 3 \cdot 10^5$, $\mathrm{Ta} = 4 \cdot 10^6$ (defined with the horizontal box extent) as functions of colatitude ϑ. Symbols: values for $\Gamma = 0.75$ for the same Ta.

Ra is apparently not yet reached. In any case, the coefficients are not drastically influenced by the Rayleigh number.

Nevertheless it seems worth a try to remove the Ra dependence of the $C_{1,6,7}$ completely by reinstating the diffusive terms parametrized by the $C_{\nu,\nu\chi,\chi}$ in the closure. In doing so, we rename the Ra dependent C_i, obtained as described before under the assumption of vanishing diffusion, by labelling them with a prime and set according to Eqs. (21) – (23)

$$\begin{aligned} C_1' &= C_1 + \nu C_\nu/(L\sqrt{\mathcal{R}}), \\ C_6' &= C_6 + \tfrac{1}{2}(\nu+\chi) C_{\nu\chi}/(L\sqrt{\mathcal{R}}), \\ C_7' &= C_7 + \chi C_\chi/(L\sqrt{\mathcal{R}}). \end{aligned} \tag{32}$$

We note that it is not possible to write a similar expression for C_2. Hence, it must here remain Ra dependent.

Given N runs with different values of Ra, the two closure coefficients occurring in each of the equalities (32), but now being assumed to be independent of Ra, can be determined by a standard least–squares approach. In the non–rotating case we obtain in this way

$$\begin{aligned} &C_1 = 0.9, \quad C_6 = 2.7, \quad C_7 = 1.7, \\ &C_\nu = 164.7, \quad C_\chi = 101.6, \quad C_{\nu\chi} = 151.1\,. \end{aligned} \tag{33}$$

For giving an impression of the quality of the fit, these values have been employed in (32) to re–calculate the $C'_{1,6,7}$, and Fig. 8 (left) shows the results in comparison with the original Ra-dependent values. In the Ra interval studied, the assumption of Ra–independence seems well justified for C_1 and to a bit lesser degree also for C_7, but not for C_6. Figure 8 (right) presents corresponding data for the rotating case $\mathrm{Ta} = 10^6$, $\vartheta = 0$. Here, the fit is much better, but note that $N = 3$ only.

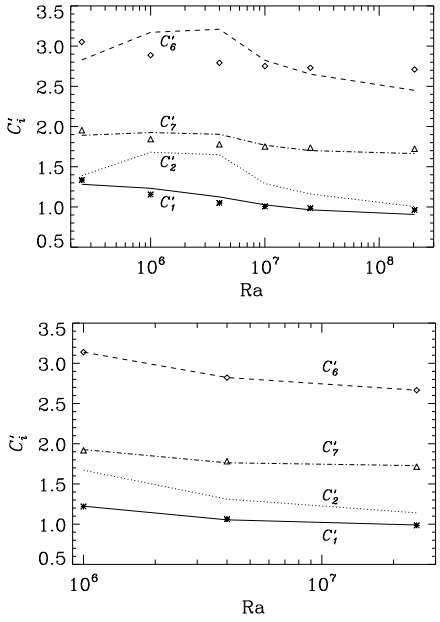

Fig. 8: Closure parameters from the least–squares fit (lines) in the cases $\mathrm{Ta} = 0$ (left) and $\mathrm{Ta} = 10^6$, $\vartheta = 0$ (right) as functions of Ra with $\mathrm{Pr} = 1$. Symbols: corresponding closure parameters $C'_{1,6,7}$ obtained from (32) with the values (33).

3.2.6 Dependence of the Nusselt on the Rayleigh number

The results for various Rayleigh numbers allow us to study the dependence of the Nusselt number Nu on Ra resulting from both the closure model and DNS. A similar exercise was done in GOMS10 for the inhomogeneous case.

From the closed–form solution (B6) of the closure model one can derive the asymptotic behavior of $\mathrm{Nu}(\mathrm{Ra})$ for $\mathrm{Ra} \to \infty$ in the cases $\mathbf{\Omega} = \mathbf{0}$ or $\vartheta = 0$. Replacing the constants $C_{1,6,7}$ in (B6) according to (32) and assuming the Prandtl number to be finite and independent of Ra, it can be seen that the only consistent assumption for $\mathcal{R}$ in this limit is $\mathcal{R} = \text{const}$. Then we have from (18) and (B7) the relation $\mathrm{Nu}(\mathrm{Ra}) \sim \mathrm{Ra}^{1/2}$ for $\mathrm{Ra} \to \infty$ as expected. The same scaling was obtained in Calzavarini et al. (2005).

In order to compare the closure model results with the numerical ones we need to require $C_{\nu,\nu\chi,\chi} \neq 0$. Otherwise, the diffusivities ν and χ would have no effect rendering the results same for all Ra. To calculate the Nusselt number

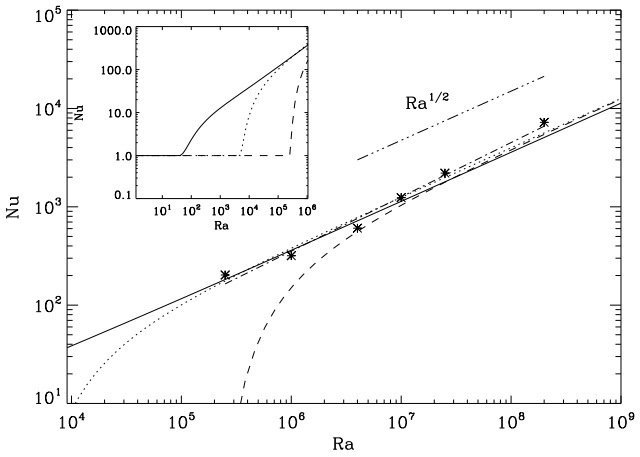

Fig. 9: Dependence of the Nusselt number on the Rayleigh number, $\mathrm{Ta} = 0$, $\mathrm{Pr} = 1$. Symbols: DNS results. Lines: results of the closure model with different model coefficients – solid: original GOMS10 values $C_{1,2,6,7} = 0.4, 0.6, 1.4, 1.4$, rescaled with $\pi^{1/2}$, $C_{\nu,\chi,\nu\chi} = 12, 6, 2$, rescaled with π; dotted: $C_{1,2,6,7} = 0.9, 1.4, 2.7, 1.7$, $C_{\nu,\chi,\nu\chi} = 164.7, 101.6, 151.1$ from (33), with C_2 taken to be the average of the values in Fig. 8; dashed: same as dotted, but $C_{\nu,\chi,\nu\chi} = 1000$ chosen arbitrarily. Dash–dotted line: power law fit $\mathrm{Nu} = 0.17 \cdot \mathrm{Ra}^{0.55}$ to the DNS data; dash–triple–dotted: $\mathrm{Nu} \sim \mathrm{Ra}^{1/2}$ asymptotics.

from the closure we use the constant (Ra–independent) values for $C_{1,6,7,\nu,\nu\chi,\chi}$ derived in Section 3.2.5, Eq. (33) while taking the average of the least–squares results for C_2 illustrated in Fig. 8.

The resulting $\mathrm{Nu}(\mathrm{Ra})$ dependence is shown in Fig. 9 together with the relation obtained with the original GOMS10 closure coefficients. To demonstrate the effect of the diffusive terms on the closure results, we have also plotted the results for the arbitrarily chosen values $C_{\nu,\chi,\nu\chi} = 1000$. One can readily see that they contribute only in the low Rayleigh number regime, especially altering the critical Ra. In the asymptotic regime, the values obtained from DNS, plotted with symbols, are in fair agreement with our closure results, and with those of GOMS10. (Note that there $L = L_x/\sqrt{\pi}$ was used in contrast to our choice $L = L_x$. This effectively means a rescaling of the closure parameters.)

Also plotted are the asymptotic $\mathrm{Nu} \propto \mathrm{Ra}^{1/2}$ (dash–triple–dotted line) and a power law fit $\mathrm{Nu} \approx 0.17\mathrm{Ra}^{0.55}$ to the DNS data, obtained with linear regression. It is worth noting that the $\mathrm{Ra}^{1/2}$ asymptotics is also produced by the closure model of Canuto et al. (1996).

3.2.7 Reynolds stress and heat fluxes in comparison to compressible simulations

The off–diagonal Reynolds stresses and the turbulent heat flux are important in generating the differential rotation of stellar convective envelopes (e.g. Rüdiger 1989). These quantities have been computed from numerous simulations of compressible convection in Cartesian (e.g. Chan 2001; Käpylä et al. 2004; Pulkkinen et al. 1993; Rüdiger et al. 2005b) and spherical geometries (e.g. Käpylä et al. 2011; Rieutord et al. 1994). It is important to compare the results of our homogeneous Boussinesq runs to those in the literature in order to draw conclusions on the robustness of certain features such as the latitude and rotation rate dependence.

We find that $\mathcal{R}_{xy}$, corresponding to latitudinal flux of angular momentum, is always positive (except in a few statistically insignificant cases), i.e. the flux is directed towards the equator in accordance with previous DNS and analytical theory (Kichatinov & Rüdiger 1993; Kitchatinov & Rüdiger 2005). There is a tendency for the maximum of $\mathcal{R}_{xy}$ to move towards the equator as the rotation rate is increased in accordance with compressible simulations of Chan (2001) and Käpylä et al. (2004). Furthermore, the vertical flux corresponding to $\mathcal{R}_{yz}$ is always negative. No sign reversal, observed at high Co in compressible runs of Käpylä et al. (2004), is seen here even for the highest Taylor numbers. The third off–diagonal component $\mathcal{R}_{xz}$ is negative for $\mathrm{Ta} \leq 2.56 \cdot 10^6$, whereas positive values occur first at mid-latitudes for $\mathrm{Ta} = 5.76 \cdot 10^6$ and at progressively higher latitudes as the rotation is increased. Earlier results suggest a similar qualitative behavior (e.g. Pulkkinen et al. 1993).

Apart from the equator, the latitudinal heat flux $\mathcal{F}_x$ is always directed towards the pole; except for the highest Taylor numbers, the azimuthal heat flux $\mathcal{F}_y$ is always negative, except for a few cases at the pole, i.e. in the retrograde direction. These features are broadly in accordance with Cartesian (e.g. Rüdiger et al. 2005a) and spherical simulations (e.g. Käpylä et al. 2011). One puzzling feature of our simulations is the monotonously increasing $\mathcal{F}_z$ at the pole as a function of Taylor number, see Table C1. At all other colatitudes $\mathcal{F}_z$ has a minimum at $\mathrm{Ta} = 1.44 \cdot 10^6 \ldots 1.6 \cdot 10^7$. We also note that $\mathcal{R}_{xz}$ and $\mathcal{F}_x$ obtain values of the order of $\mathcal{R}_{xx}$ and $\mathcal{F}_z$, for Taylor numbers $10^8 \ldots 10^{10}$ and 10^{10}, respectively, at latitudes $15^\circ \ldots 45^\circ$. In some of these cases the flow structures are rather laminar which may reflect the fact that convection is only mildly supercritical. The large values of $\mathcal{R}_{zz}$, $\mathcal{F}_z$ and $\mathcal{Q}$ at the pole for the highest Ta might be explainable by a strong dominance of the elevator modes if the secondary instabilities which are limiting their growth are suppressed by rapid rotation.

4 Conclusions

The closure presented in GOMS10 has been known not to reproduce essential flow features under rotation, at least when the rotation and gravity vectors are aligned. In this study we made an attempt to extend the applicability of the model in the presence of rotation by allowing the model parameters to depend on the rotation rate (or Taylor number). A similar modification to the GOMS10 model can be found

in Miller & Garaud (2007), where the length scale L was assumed to vary as a function of the rotation rate. Our approach is more general because it allows the model parameters to obey individual dependences on Ta.

The main conclusion to be drawn from our investigations with the homogeneous Boussinesq closure model is that the envisaged extension works perfectly at the pole, while elsewhere the validity of the closure degrades at first when rotation rate and colatitude are increased, as indicated by the growing residuals of the parameter fits (see Figs. 3 and 5). For even higher rotation rates, however, the closure validity recovers again. This suggests that even this modified GOMS10 closure is essentially incomplete for intermediate rotation rates. In particular, given the clear anisotropy induced by the direction of rotation, the purely isotropizing character of the closure ansatz should be revised.

However, even in the non–rotating case we were not able to reproduce the ratios of the coefficients C_i provided in GOMS10, see Table 2. Increasing the Rayleigh number in the DNS runs did not solve this issue. This might be attributed to the fact that the coefficients in that study were not independently determined from DNS, but instead adopted without change from the inhomogeneous model while only adjusting the length scale L.

We observed that positivity of the parameters and their adherence to the realizability condition alone always guarantee stability of the stationary solutions of the closure model in accordance with the stability of the underlying statistically stationary DNS solution.

In this study we have only briefly explored the influence of the Rayleigh number on the optimum model coefficients. One motivation of this was to see, whether the parameters settle to some constant values with increasing Ra. Apart from some weak signs of convergence in rotating runs, we found no clear asymptotic tendencies, although the acquired parameters do not change dramatically. More systematic efforts are needed to clarify this issue. Future research should also extend the present work to other settings including bounded domains which require a one–dimensional version of the closure as already employed in GOMS10. Moreover, from our inspections the conclusion can be drawn that rotation dependent amendments would have the greatest benefit in the equations of $\mathcal{R}_{xz,yz}$ and $\mathcal{F}_x$.

We also set out to investigate the effect of changing the aspect ratio of the computational domain. As a result, only a weak dependence was found in any other latitudinal location than the pole. Even at the pole and with aspect ratio unity, these modes are subject to parasitic instabilities that eventually suppress them, having yet a noticeable influence on the turbulence.

Acknowledgements. The computations were performed on the facilities hosted by the CSC – IT Center for Science in Espoo, Finland, who are financed by the Finnish ministry of education, and on the FGI and Helsinki University cluster 'Alcyone'. The authors acknowledge financial support from the Academy of Finland grant Nos. 136189, 140970, 272786 (PJK), Centre of Excellence ReSoLVE, grant No. 272157 (MJK, PJK), and the University of Helsinki research project 'Active Suns'. The authors acknowledge the hospitality of NORDITA. JES acknowledges the financial support from the Finnish Cultural Foundation. We thank Elizabeth Cole for help in improving the language.

A Closure model equations for the inhomogeneous Boussinesq system

Here we describe the closure model for the general inhomogeneous case of Boussinesq convection, first without restricting to a specific mean. Evolution equations for the Reynolds stress and turbulent heat flux can be derived from the equations for the fluctuating quantities $\boldsymbol{u}$ and θ. These read

$$\begin{aligned}\frac{\partial \boldsymbol{u}}{\partial t} =& -\overline{\boldsymbol{U}}\cdot\boldsymbol{\nabla}\boldsymbol{u}-\boldsymbol{u}\cdot\boldsymbol{\nabla}\overline{\boldsymbol{U}}-\alpha\theta\boldsymbol{g}-\boldsymbol{\nabla}\psi\\ &-2\,\boldsymbol{\Omega}\times\boldsymbol{u}+\nu\boldsymbol{\nabla}^2\boldsymbol{u}-\boldsymbol{\nabla}\cdot(\boldsymbol{u}\otimes\boldsymbol{u}-\boldsymbol{\mathcal{R}}),\qquad\text{(A1)}\\ \frac{\partial\theta}{\partial t} =& -\overline{\boldsymbol{U}}\cdot\boldsymbol{\nabla}\theta-\boldsymbol{u}\cdot(\boldsymbol{\nabla}\overline{\Theta}+\boldsymbol{G}_0)+\chi\boldsymbol{\nabla}^2\theta-\boldsymbol{\nabla}\cdot(\theta\boldsymbol{u}-\boldsymbol{\mathcal{F}}),\end{aligned}$$

with $\otimes$ denoting the dyadic product and $\boldsymbol{G}_0=\boldsymbol{\nabla}T_0-\boldsymbol{g}/c_p$. For the Reynolds stress $\mathcal{R}_{ij}$, the turbulent heat flux $\mathcal{F}_i$ and the temperature variance $\mathcal{Q}$ we obtain

$$\begin{aligned}&\dot{\mathcal{R}}_{ij}+\overline{U}_k\partial_k\mathcal{R}_{ij}+\mathcal{R}_{ik}\partial_k\overline{U}_j+\mathcal{R}_{jk}\partial_k\overline{U}_i+\alpha(\mathcal{F}_ig_j+\mathcal{F}_jg_i)\\ &\quad-\nu\partial_{kk}\mathcal{R}_{ij}+2\Omega_l(\varepsilon_{ilk}\mathcal{R}_{jk}+\varepsilon_{jlk}\mathcal{R}_{ik})\qquad\text{(A2)}\\ &=-\overline{u_i\partial_j\psi+u_j\partial_i\psi}-\overline{u_i\partial_k(u_ju_k)+u_j\partial_k(u_iu_k)}\\ &\quad-2\nu\,\overline{\partial_ku_i\partial_ku_j},\\ &\dot{\mathcal{F}}_i+\overline{U}_j\partial_j\mathcal{F}_i+\mathcal{F}_j\partial_j\overline{U}_i+\mathcal{R}_{ij}(\partial_j\overline{\Theta}+G_{0j})+\alpha\mathcal{Q}g_i\\ &\quad-\tfrac{1}{2}(\nu+\chi)\partial_{jj}\mathcal{F}_i+2\varepsilon_{ijk}\Omega_j\mathcal{F}_k\qquad\text{(A3)}\\ &=-\overline{\theta\partial_i\psi}-\overline{\theta\partial_j(u_iu_j)+u_i\partial_j(\theta u_j)}\\ &\quad+\tfrac{1}{2}(\nu-\chi)\overline{\partial_k(\theta\partial_ku_i-u_i\partial_k\theta)}-(\nu+\chi)\overline{\partial_k\theta\partial_ku_i},\\ &\dot{\mathcal{Q}}+\overline{U}_i\partial_i\mathcal{Q}+2\mathcal{F}_i(\partial_i\overline{\Theta}+G_{0i})-\chi\partial_{ii}\mathcal{Q}\qquad\text{(A4)}\\ &=-2\overline{\theta\partial_i(\theta u_i)}-2\chi\overline{(\partial_i\theta)^2}.\end{aligned}$$

Here, the right hand sides contain third–order correlations of fluctuating quantities (including the correlations with the pressure ψ) and terms originating from the Laplacians which cannot be expressed by the considered second–order correlations. In the closure model of GOMS10 all these are replaced in the following way:

$$\begin{aligned}&\overline{u_i\partial_j\psi+u_j\partial_i\psi}+\overline{u_i\partial_k(u_ju_k)+u_j\partial_k(u_iu_k)}\qquad\text{(A5)}\\ &+2\nu\overline{\partial_ku_i\partial_ku_j}\to\frac{C_1}{L}\mathcal{R}^{1/2}\mathcal{R}_{ij}+\frac{C_2}{L}\mathcal{R}^{1/2}(\mathcal{R}_{ij}-\tfrac{1}{3}\mathcal{R}\delta_{ij})\\ &\qquad+\nu\frac{C_\nu}{L^2}\mathcal{R}_{ij}=\Lambda_{\mathcal{R}}\mathcal{R}_{ij}-\frac{C_2}{3L}\mathcal{R}^{3/2}\delta_{ij},\end{aligned}$$

$$\overline{\theta\partial_i\psi} + \overline{\theta\partial_j(u_iu_j) + u_i\partial_j(\theta u_j)} - \tfrac{1}{2}(\nu-\chi)\overline{\partial_k(\theta\partial_k u_i - u_i\partial_k\theta)} + (\nu+\chi)\overline{\partial_k\theta\partial_k u_i} \to \frac{C_6}{L}\mathcal{R}^{1/2}\mathcal{F}_i + \tfrac{1}{2}(\nu+\chi)\frac{C_{\nu\chi}}{L^2}\mathcal{F}_i = \Lambda_{\mathcal{F}}\mathcal{F}_i, \tag{A6}$$

$$2\big(\overline{\theta\partial_i(\theta u_i)} + \chi\overline{(\partial_i\theta)^2}\big) \to \frac{C_7}{L}\mathcal{R}^{1/2}\mathcal{Q} + \chi\frac{C_\chi}{L^2}\mathcal{Q} = \Lambda_{\mathcal{Q}}\mathcal{Q}, \tag{A7}$$

with

$$\Lambda_{\mathcal{R}} = \frac{(C_1+C_2)}{L}\mathcal{R}^{1/2} + \nu\frac{C_\nu}{L^2}, \tag{A8}$$
$$\Lambda_{\mathcal{F}} = \frac{C_6}{L}\mathcal{R}^{1/2} + \tfrac{1}{2}(\nu+\chi)\frac{C_{\nu\chi}}{L^2},\ \Lambda_{\mathcal{Q}} = \frac{C_7}{L}\mathcal{R}^{1/2} + \chi\frac{C_\chi}{L^2}.$$

Thus, the closure consists of relaxation terms, $\sim\ \mathcal{R}_{ij}$, isotropization terms $\sim\ (\mathcal{R}_{ij} - \frac{1}{3}\mathcal{R}\delta_{ij})$ and terms like $\nu C_\nu L^{-2}\mathcal{R}_{ij}$ corresponding to diffusion. For the length scale L, the distance to the closest boundary is adopted, making the closure coefficients explicitly position dependent. Applying the above ansatzes we arrive at the equations

$$\dot{\mathcal{R}}_{ij} + \overline{U}_k\partial_k\mathcal{R}_{ij} + \mathcal{R}_{ik}\partial_k\overline{U}_j + \mathcal{R}_{jk}\partial_k\overline{U}_i - \nu\partial_{kk}\mathcal{R}_{ij} + \alpha(\mathcal{F}_ig_j + \mathcal{F}_jg_i) + 2\Omega_l(\varepsilon_{ilk}\mathcal{R}_{jk} + \varepsilon_{jlk}\mathcal{R}_{ik}) = -\left(\frac{C_1+C_2}{L}\mathcal{R}^{1/2} + \nu\frac{C_\nu}{L^2}\right)\mathcal{R}_{ij} + \frac{C_2}{3L}\mathcal{R}^{3/2}\delta_{ij}, \tag{A9}$$

$$\dot{\mathcal{F}}_i + \overline{U}_j\partial_j\mathcal{F}_i + \mathcal{F}_j\partial_j\overline{U}_i + \mathcal{R}_{ij}(\partial_j\overline{\Theta} + G_{0j}) + \alpha\mathcal{Q}g_i - \tfrac{1}{2}(\nu+\chi)\partial_{jj}\mathcal{F}_i + 2\varepsilon_{ijk}\Omega_j\mathcal{F}_k = -\left(\frac{C_6}{L}\mathcal{R}^{1/2} + \tfrac{1}{2}(\nu+\chi)\frac{C_{\nu\chi}}{L^2}\right)\mathcal{F}_i, \tag{A10}$$

$$\dot{\mathcal{Q}} + \overline{U}_i\partial_i\mathcal{Q} + 2\mathcal{F}_i(\partial_i\overline{\Theta} + G_{0i}) - \chi\partial_{ii}\mathcal{Q} = -\left(\frac{C_7}{L}\mathcal{R}^{1/2} + \chi\frac{C_\chi}{L^2}\right)\mathcal{Q}. \tag{A11}$$

Assuming now periodicity in the x and y directions we define the mean suitably as the average over x and y, $\overline{f}(z) = \int_{L_x}\int_{L_y} f(x,y,z)\,dxdy/L_xL_y$. Horizontal derivatives vanish and the continuity equation reduces to $\partial_z\overline{U}_z = 0$, hence $\overline{U}_z = $ const. For a plane layer with impenetrable boundaries this yields $\overline{U}_z = 0$. With gravity in z direction, the equations for the remaining components of the mean velocity read

$$\dot{\overline{U}}_x = -\partial_z\mathcal{R}_{xz} + 2\Omega_z\overline{U}_y + \nu\partial_{zz}\overline{U}_x,$$
$$\dot{\overline{U}}_y = -\partial_z\mathcal{R}_{yz} - 2\Omega_z\overline{U}_x + \nu\partial_{zz}\overline{U}_y. \tag{A12}$$

Note that we do not need to solve for the mean reduced pressure $\overline{\Psi}$ as it does only affect $\overline{U}_z$. The equation for $\overline{\Theta}$ reduces to

$$\dot{\overline{\Theta}} = \chi\partial_{zz}\overline{\Theta} - \partial_z\mathcal{F}_z. \tag{A13}$$

For Eqs. (A9)–(A11) we have now (with $\overline{U}_z = 0$, $g = g_z$)

$$\dot{\mathcal{R}}_{xx} = -2\mathcal{R}_{xz}\partial_z\overline{U}_x + 4\Omega_z\mathcal{R}_{xy} + \nu\partial_{zz}\mathcal{R}_{xx} - \Lambda_{\mathcal{R}}\mathcal{R}_{xx} + \frac{C_2}{3L}\mathcal{R}^{3/2}, \tag{A14}$$

$$\dot{\mathcal{R}}_{xy} = -\mathcal{R}_{xz}\partial_z\overline{U}_y - \mathcal{R}_{yz}\partial_z\overline{U}_x + 2\Omega_x\mathcal{R}_{xz} + 2\Omega_z(\mathcal{R}_{yy} - \mathcal{R}_{xx}) + \nu\partial_{zz}\mathcal{R}_{xy} - \Lambda_{\mathcal{R}}\mathcal{R}_{xy}, \tag{A15}$$

$$\dot{\mathcal{R}}_{xz} = -\mathcal{R}_{zz}\partial_z\overline{U}_x - \alpha\mathcal{F}_xg - 2\Omega_x\mathcal{R}_{xy} + 2\Omega_z\mathcal{R}_{yz} + \nu\partial_{zz}\mathcal{R}_{xz} - \Lambda_{\mathcal{R}}\mathcal{R}_{xz}, \tag{A16}$$

$$\dot{\mathcal{R}}_{yy} = -2\mathcal{R}_{yz}\partial_z\overline{U}_y + 4\Omega_x\mathcal{R}_{yz} - 4\Omega_z\mathcal{R}_{xy} + \nu\partial_{zz}\mathcal{R}_{yy} - \Lambda_{\mathcal{R}}\mathcal{R}_{yy} + \frac{C_2}{3L}\mathcal{R}^{3/2}, \tag{A17}$$

$$\dot{\mathcal{R}}_{yz} = -\mathcal{R}_{zz}\partial_z\overline{U}_y - \alpha\mathcal{F}_yg + 2\Omega_x(\mathcal{R}_{zz} - \mathcal{R}_{yy}) - 2\Omega_z\mathcal{R}_{xz} + \nu\partial_{zz}\mathcal{R}_{yz} - \Lambda_{\mathcal{R}}\mathcal{R}_{yz}, \tag{A18}$$

$$\dot{\mathcal{R}}_{zz} = -2\alpha\mathcal{F}_zg - 4\Omega_x\mathcal{R}_{yz} + \nu\partial_{zz}\mathcal{R}_{zz} - \Lambda_{\mathcal{R}}\mathcal{R}_{zz} + \frac{C_2}{3L}\mathcal{R}^{3/2}, \tag{A19}$$

$$\dot{\mathcal{F}}_x = -\mathcal{R}_{xz}(\partial_z\overline{\Theta} + G_0) - \mathcal{F}_z\partial_z\overline{U}_x + \tfrac{1}{2}(\nu+\chi)\partial_{zz}\mathcal{F}_x + 2\Omega_z\mathcal{F}_y - \Lambda_{\mathcal{F}}\mathcal{F}_x, \tag{A20}$$

$$\dot{\mathcal{F}}_y = -\mathcal{R}_{yz}(\partial_z\overline{\Theta} + G_0) - \mathcal{F}_z\partial_z\overline{U}_y + \tfrac{1}{2}(\nu+\chi)\partial_{zz}\mathcal{F}_y + 2\Omega_x\mathcal{F}_z - 2\Omega_z\mathcal{F}_x - \Lambda_{\mathcal{F}}\mathcal{F}_y, \tag{A21}$$

$$\dot{\mathcal{F}}_z = -\mathcal{R}_{zz}(\partial_z\overline{\Theta} + G_0) - \alpha\mathcal{Q}g + \tfrac{1}{2}(\nu+\chi)\partial_{zz}\mathcal{F}_z - 2\Omega_x\mathcal{F}_y - \Lambda_{\mathcal{F}}\mathcal{F}_z, \tag{A22}$$

$$\dot{\mathcal{Q}} = -2\mathcal{F}_z(\partial_z\overline{\Theta} + G_0) + \chi\partial_{zz}\mathcal{Q} - \Lambda_{\mathcal{Q}}\mathcal{Q}\,. \tag{A23}$$

with $G_0 = G_{0z}$. Note that the stationary version of the autonomous system (A12)–(A23) does have non–trivial solutions as demonstrated in GOMS10. Due to the nonlinearity of the system they exist not only for specific combinations of its parameters like in linear eigenvalue problems, but (at least within wide margins) for any specification of them.

For $\Omega_x = 0$, that is, at the pole, there is a special stationary solution of the system (A12)–(A23) characterized by $\overline{U}_{x,y} = \mathcal{R}_{xy,xz,yz} = \mathcal{F}_{x,y} = 0$, $\mathcal{R}_{xx} = \mathcal{R}_{yy}$ which is not explicitly dependent on Ω_z and hence identical with the corresponding solution of the non–rotating case.

B Closure model equations for the homogeneous Boussinesq system

In this case we redefine the average as a volume rather than a horizontal one, making the mean quantities indepedent of

z, and obtain

$$\begin{aligned}
\dot{\mathcal{R}}_{xx} &= 4\Omega_z\mathcal{R}_{xy} - \Lambda_\mathcal{R}\mathcal{R}_{xx} + \frac{C_2}{3L}\mathcal{R}^{3/2},\\
\dot{\mathcal{R}}_{xy} &= 2\Omega_x\mathcal{R}_{xz} + 2\Omega_z(\mathcal{R}_{yy} - \mathcal{R}_{xx}) - \Lambda_\mathcal{R}\mathcal{R}_{xy},\\
\dot{\mathcal{R}}_{xz} &= -\alpha\mathcal{F}_x g - 2\Omega_x\mathcal{R}_{xy} + 2\Omega_z\mathcal{R}_{yz} - \Lambda_\mathcal{R}\mathcal{R}_{xz},\\
\dot{\mathcal{R}}_{yy} &= 4\Omega_x\mathcal{R}_{yz} - 4\Omega_z\mathcal{R}_{xy} - \Lambda_\mathcal{R}\mathcal{R}_{yy} + \frac{C_2}{3L}\mathcal{R}^{3/2},\\
\dot{\mathcal{R}}_{yz} &= -\alpha\mathcal{F}_y g + 2\Omega_x(\mathcal{R}_{zz} - \mathcal{R}_{yy}) - 2\Omega_z\mathcal{R}_{xz} - \Lambda_\mathcal{R}\mathcal{R}_{yz},\\
\dot{\mathcal{R}}_{zz} &= -2\alpha\mathcal{F}_z g - 4\Omega_x\mathcal{R}_{yz} - \Lambda_\mathcal{R}\mathcal{R}_{zz} + \frac{C_2}{3L}\mathcal{R}^{3/2},\\
\dot{\mathcal{F}}_x &= -\mathcal{R}_{xz}G_0 + 2\Omega_z\mathcal{F}_y - \Lambda_\mathcal{F}\mathcal{F}_x,\\
\dot{\mathcal{F}}_y &= -\mathcal{R}_{yz}G_0 + 2\Omega_x\mathcal{F}_z - 2\Omega_z\mathcal{F}_x - \Lambda_\mathcal{F}\mathcal{F}_y,\\
\dot{\mathcal{F}}_z &= -\mathcal{R}_{zz}G_0 - \alpha\mathcal{Q}g - 2\Omega_x\mathcal{F}_y - \Lambda_\mathcal{F}\mathcal{F}_z,\\
\dot{\mathcal{Q}} &= -2\mathcal{F}_z G_0 - \Lambda_\mathcal{Q}\mathcal{Q},
\end{aligned} \tag{B1}$$

which is for $\mathbf{\Omega} = \mathbf{0}$ equivalent to Eqs. (53) of GOMS10. The resulting equation for $\mathcal{R}$ reads

$$\dot{\mathcal{R}} = -2\alpha\mathcal{F}_z g - \frac{C_1}{L}\mathcal{R}^{3/2} \tag{B2}$$

and is not explicitly influenced by rotation.

B.1 Solutions

In the non–rotating case the equations for $\dot{\mathcal{R}}_{xx}$, $\dot{\mathcal{R}}_{yy}$, $\dot{\mathcal{R}}_{zz}$, $\dot{\mathcal{F}}_z$ and $\dot{\mathcal{Q}}$ form a closed system which can be solved in separation from the remaining equations. Once the solution of the former is known the latter can be solved where one finds again two separate systems: $\{\dot{\mathcal{R}}_{xz}, \dot{\mathcal{F}}_x\}$ and $\{\dot{\mathcal{R}}_{yz}, \dot{\mathcal{F}}_y\}$. They have the same shape, and when assuming that there is a stationary solution for $\mathcal{R}$ from the first system, we arrive at the eigenvalue problem for the growth rate of an ansatz $\mathcal{R}_{xz}, \mathcal{F}_x, \mathcal{R}_{yz}, \mathcal{F}_y \sim \exp(\lambda t)$

$$\begin{vmatrix} \Lambda_\mathcal{R} + \lambda & \alpha g \\ G_0 & \Lambda_\mathcal{F} + \lambda \end{vmatrix} = 0 \tag{B3}$$

with constant $\Lambda_\mathcal{R}, \Lambda_\mathcal{F}$. The solutions are

$$\lambda_{1,2} = -\frac{\Lambda_\mathcal{R} + \Lambda_\mathcal{F}}{2} \pm \sqrt{\frac{(\Lambda_\mathcal{R} - \Lambda_\mathcal{F})^2}{4} + \alpha g G_0} \tag{B4}$$

and given that $\alpha g G_0 > 0$ for convection, unstable solutions cannot completely be ruled out for sufficiently large values of this product, but had most likely to be considered unphysical.

Nontrivial closed form *stationary* solutions can be derived for the special settings $\mathbf{\Omega} = \mathbf{0}$ or $\vartheta = 0$ (pole): In both cases we have as in the inhomogeneous case

$$\mathcal{R}_{xy,xz,yz} = \mathcal{F}_{x,y} = 0, \quad \mathcal{R}_{xx,yy} = \frac{C_2}{3(C_1 + C_2)}\mathcal{R} \tag{B5}$$

hence

$$\mathcal{R} = \frac{2\alpha g G_0 L^2}{C_1 C_6}\left(\frac{C_1}{C_7} + \frac{3C_1 + C_2}{3(C_1 + C_2)}\right) \tag{B6}$$

$$\mathcal{R}_{zz} = \frac{3C_1 + C_2}{3(C_1 + C_2)}\mathcal{R}, \quad \mathcal{F}_z = -\frac{C_1}{2\alpha g L}\mathcal{R}^{3/2} \tag{B7}$$

$$\mathcal{Q} = \frac{G_0}{\alpha g}\frac{C_1}{C_7}\mathcal{R} \tag{B8}$$

which coincides with the solution given in GOMS10. In turn it is under these conditions possible to determine the C_i uniquely when $\mathcal{R}_{xx} = \mathcal{R}_{yy}$, $\mathcal{R}_{zz}$, $\mathcal{F}_z$ and $\mathcal{Q}$ are given from a DNS:

$$\begin{aligned}
3\mathcal{R}_{xx}C_1 - (\mathcal{R}_{zz} - \mathcal{R}_{xx})\,C_2 &= 0\\
3\mathcal{R}_{zz}C_1 + (3\mathcal{R}_{zz} - \mathcal{R})C_2 &= -6\alpha g L\mathcal{F}_z/\mathcal{R}^{1/2}\\
C_6 &= -(G_0\mathcal{R}_{zz} + \alpha g\mathcal{Q})L/\mathcal{F}_z\mathcal{R}^{1/2}\\
C_7 &= -2G_0 L\mathcal{F}_z/\mathcal{Q}\mathcal{R}^{1/2}.
\end{aligned} \tag{B9}$$

Inserting (B6) in (B4) we obtain

$$\begin{aligned}
&(\Lambda_\mathcal{R} - \Lambda_\mathcal{F})^2 + 4\alpha g G_0 - (\Lambda_\mathcal{R} + \Lambda_\mathcal{F})^2 \qquad \text{(B10)}\\
&= 4(\alpha g G_0 - \Lambda_\mathcal{R}\Lambda_\mathcal{F}) = 2\alpha g G_0\left(1 - \frac{C_1 + C_2}{C_7} - \frac{C_2}{3C_1}\right)
\end{aligned}$$

the sign of which depends solely on the parameters C_i and not on $\alpha g G_0$. Requiring (B10) to be negative for stability provides an additional constraint. A corresponding generalized condition, ensuring overall stability, is referred to in Sec. 3.2.2.

Another special situation is found at the equator ($\vartheta = 90°$, hence $\Omega_z = 0$) where the system (B1) decomposes into a closed one for the quantities $\mathcal{R}_{xx}$, $\mathcal{R}_{yy}$, $\mathcal{R}_{yz}$, $\mathcal{R}_{zz}$, $\mathcal{F}_y$, $\mathcal{F}_z$ and $\mathcal{Q}$ and another one for $\mathcal{R}_{xy}$, $\mathcal{R}_{xz}$ and $\mathcal{F}_x$ which can be solved once $\mathcal{R}$ from the first system is known. The latter reads in the stationary case

$$\begin{aligned}
0 &= 2\Omega_x\mathcal{R}_{xz} - \Lambda_\mathcal{R}\mathcal{R}_{xy},\\
0 &= -\alpha\mathcal{F}_x g - 2\Omega_x\mathcal{R}_{xy} - \Lambda_\mathcal{R}\mathcal{R}_{xz},\\
0 &= -\mathcal{R}_{xz}G_0 - \Lambda_\mathcal{F}\mathcal{F}_x,
\end{aligned}$$

where $\mathcal{F}_x$ can be eliminated by the last line. The remaining two equations form a homogeneous linear system for $\mathcal{R}_{xy}$ and $\mathcal{R}_{xz}$ having the determinant

$$\alpha g G_0\frac{C_1 + C_2}{C_6} - \left(\frac{C_1 + C_2}{L}\right)^2\mathcal{R} - 4\Omega_x^2.$$

Nontrivial solutions would be possible if $\mathcal{R}$ were to assume a special value depending on the parameters. However, this has the unphysical consequence of $\mathcal{R}_{xy}$, $\mathcal{R}_{xz}$ and $\mathcal{F}_x$ becoming dependent on an arbitrary quantity. So we have to conclude, that they either vanish or are time–dependent. In the latter case we have to require stability, so these quantities were bound to decay to zero or to perform stationary

oscillations with an arbitrary amplitude. As the only physically meaningful option we assume that they vanish. The remaining system reads

$$
\begin{aligned}
0 &= -\Lambda_{\mathcal{R}}\mathcal{R}_{xx} + \frac{C_2}{3L}\mathcal{R}^{3/2},\\
0 &= 4\Omega_x\mathcal{R}_{yz} - \Lambda_{\mathcal{R}}\mathcal{R}_{yy} + \frac{C_2}{3L}\mathcal{R}^{3/2},\\
0 &= -\alpha\mathcal{F}_y g + 2\Omega_x(\mathcal{R}_{zz} - \mathcal{R}_{yy}) - \Lambda_{\mathcal{R}}\mathcal{R}_{yz},\\
0 &= -2\alpha\mathcal{F}_z g - 4\Omega_x\mathcal{R}_{yz} - \Lambda_{\mathcal{R}}\mathcal{R}_{zz} + \frac{C_2}{3L}\mathcal{R}^{3/2},\\
0 &= -\mathcal{R}_{yz}G_0 + 2\Omega_x\mathcal{F}_z - \Lambda_{\mathcal{F}}\mathcal{F}_y,\\
0 &= -\mathcal{R}_{zz}G_0 - \alpha\mathcal{Q}g - 2\Omega_x\mathcal{F}_y - \Lambda_{\mathcal{F}}\mathcal{F}_z,\\
0 &= -2\mathcal{F}_z G_0 - \Lambda_{\mathcal{Q}}\mathcal{Q}.
\end{aligned}
$$

From the first line it follows $\mathcal{R} = C_{12}(\mathcal{R}_{yy} + \mathcal{R}_{zz})$, $C_{12} = 3(C_1+C_2)/(3C_1+2C_2)$, from the last $\mathcal{Q} = -2G_0\mathcal{F}_z/\Lambda_{\mathcal{Q}}$ leaving a system with five variables only. It can be broken down to a nonlinear equation for $\mathcal{R}$ which is (apart from $\mathcal{R} = 0$) solved by the solutions of

$$
2\Omega_x\big(2K - \frac{\mathcal{R}E(\mathcal{R})}{C_{12}}\big) - \Lambda_{\mathcal{R}}KD(\mathcal{R}) - \alpha g G(\mathcal{R})E(\mathcal{R}) = 0, \tag{B11}
$$

completed by

$$
\begin{aligned}
&\mathcal{F}_z = K\mathcal{R}^{3/2}, \quad \mathcal{F}_y = G(\mathcal{R})\mathcal{R}^{3/2}, \quad K = -C_1/L,\\
&\mathcal{R}_{yy} = \frac{\mathcal{R}}{C_{12}} - \frac{K}{E(\mathcal{R})}\mathcal{R}^{3/2}, \quad \mathcal{R}_{yz} = \frac{KD(\mathcal{R})}{E(\mathcal{R})}\mathcal{R}^{3/2},\\
&\mathcal{R}_{zz} = \frac{K}{E(\mathcal{R})}\mathcal{R}^{3/2},
\end{aligned}
$$

with

$$
\begin{aligned}
E(\mathcal{R}) &= A_z D + B_z,\ G(\mathcal{R}) = \frac{1}{K}\frac{A_z D + B_z}{A_y D + B_y}\\
D(\mathcal{R}) &= \alpha g \frac{4\Omega_x B_z + \Lambda_{\mathcal{R}} B_y}{16\Omega_x^2 + \Lambda_{\mathcal{R}}^2 - \alpha g\big(4\Omega_x A_z - \Lambda_{\mathcal{R}} A_y\big)}\\
A_y(\mathcal{R}) &= \frac{G_0}{\Delta}(\alpha g G_0/\Lambda_{\mathcal{Q}} - \Lambda_{\mathcal{F}}),\\
B_y(\mathcal{R}) &= -G_0 2\Omega_x/\Delta = -A_z,\ B_z(\mathcal{R}) = -G_0\Lambda_{\mathcal{F}}/\Delta,\\
\Delta(\mathcal{R}) &= 4\Omega_x^2 + \Lambda_{\mathcal{F}}(\Lambda_{\mathcal{F}} - \alpha g 2G_0/\Lambda_{\mathcal{Q}}).
\end{aligned}
$$

It cannot be guaranteed that (B11) has positive solutions for $\mathcal{R}$ for any arbitrary set of parameters, in particular for arbitrary positive C_i.

In contrast, for $\mathbf{\Omega} \neq \mathbf{0}$ and $\vartheta \neq 0, 90^\circ$ none of the components of $\boldsymbol{\mathcal{R}}$ and $\boldsymbol{\mathcal{F}}$ disappear.

B.2 Realizability constraint

With respect to the realizability constraint (29), an analysis analogous to that of GOMS10, App. A, but with rotation included, leads to the following relation for the temporal derivative of the quantity $\mathcal{T} = X_i T_{ij} X_j = X_i(\mathcal{R}_{ij} - \mathcal{Q}^{-1}\mathcal{F}_i\mathcal{F}_j)X_j$

$$
\begin{aligned}
\partial_t\mathcal{T} = &(2C_6 - C_7 - C_1 - C_2)(\boldsymbol{\mathcal{F}}\cdot\boldsymbol{X})^2\frac{\sqrt{\mathcal{R}}}{\mathcal{Q}L}\\
&+ \frac{C_2}{3L}\mathcal{R}^{3/2}\boldsymbol{X}^2 - (C_1+C_2)\frac{\mathcal{T}\sqrt{\mathcal{R}}}{L}\\
&+ 2(\boldsymbol{\mathcal{F}}\cdot\boldsymbol{X})\mathcal{Q}^{-1}X_j T_{jz}G_0 - 4X_i\varepsilon_{ilk}\Omega_l T_{jk}X_j.
\end{aligned} \tag{B12}
$$

Repeating the arguments of GOMS10 here, one finds that the realizability condition is not affected by the presence of rotation, since Ω_l in (B12) is multiplied by the vanishing term $T_{ij}X_j$. Similarly, by retaining the model coefficients C_ν, C_κ and $C_{\nu\kappa}$ one can derive the following expression

$$
\begin{aligned}
\partial_t\mathcal{T} = &\Big(2C_6 - C_7 - C_1 - C_2\\
&+ \frac{2(\nu+\kappa)C_{\nu\kappa} - \kappa C_\kappa - \nu C_\nu}{L\sqrt{\mathcal{R}}}\Big)(\boldsymbol{\mathcal{F}}\cdot\boldsymbol{X})^2\frac{\sqrt{\mathcal{R}}}{\mathcal{Q}L}\\
&+ \frac{C_2}{3L}\mathcal{R}^{3/2}\boldsymbol{X}^2 - (C_1+C_2)\frac{\mathcal{T}\sqrt{\mathcal{R}}}{L}\\
&+ 2(\boldsymbol{\mathcal{F}}\cdot\boldsymbol{X})\mathcal{Q}^{-1}X_j T_{jz}G_0 - 4X_i\varepsilon_{ilk}\Omega_l T_{jk}X_j\\
&- X_i\frac{\nu C_\nu}{L^2}T_{ij}X_j\,,
\end{aligned}
$$

from which one obtains the realizability criterion

$$
2C_6 - C_7 - C_1 - C_2 + \frac{2(\nu+\kappa)C_{\nu\kappa} - \kappa C_\kappa - \nu C_\nu}{L\sqrt{\mathcal{R}}} \geq 0.
$$

This criterion cannot be formulated as a condition for the model parameters alone, unlike (29). However, we can infer the two *sufficient* conditions (29) and $2(\nu+\kappa)C_{\nu\kappa} - \kappa C_\kappa - \nu C_\nu \geq 0$. With $\mathrm{Pr} = 1$ the latter one can be written as $4C_{\nu\kappa} - C_\kappa - C_\nu \geq 0$, which is satisfied by the values $C_{\nu\kappa} \approx 6$, $C_\nu \approx 12$ and $C_\kappa \approx 2$ given in GOMS10 and also by our result (33).

C Simulation data

References

Bell, J. B. & Marcus, D. L. 1992, Journal of Computational Physics, 101, 334

Brandenburg, A. 2003, in Advances in Nonlinear Dynamics, ed. Ferriz-Mas, A. & Núñez, M. (Taylor and Francis, London), 269

Brandenburg, A. & Dobler, W. 2002, Computer Physics Communications, 147, 471

Calzavarini, E., Doering, C. R., Gibbon, J. D., et al. 2006, Physical Review E, 73, 035301

Calzavarini, E., Lohse, D., Toschi, F., & Tripiccione, R. 2005, Physics of Fluids, 17, 055107

Canuto, V. M., Goldman, I., & Mazzitelli, I. 1996, ApJ , 473, 550

Canuto, V. M. 1997, ApJ , 482, 827

Canuto, V. M. 2011, Astron. Astrophys., 528, A76

Chan, K. L. 2001, ApJ , 548, 1102

Table C1: Summary of the DNS results for $\mathrm{Ra} = 3 \cdot 10^5$, $\mathrm{Pr} = 0.6$. Normalizations (indicated by a tilde) are carried out with $\alpha g d^2 G_0$ for Reynolds stress, with $d^2 G_0^{3/2} (\alpha g)^{1/2}$ for heat flux, and with $(dG_0)^2$ for temperature variance. The grid size in all runs in Sets Z and A–G is 64^3 for the lower rotation rates and 128^3 or 144^3 for the higher ones. A few spot checks at 256^3 confirmed convergence. However, see Sec. 3.1 for the convergence issue related to the time step. In the Runs indicated by bullets viscous heating was included, see Sec. 2.1.1.

Run	ϑ	Ta $[10^6]$	Co	Re	$\tilde{\mathcal{R}}_{xx}$	$\tilde{\mathcal{R}}_{xy}$ $[10^{-2}]$	$\tilde{\mathcal{R}}_{xz}$ $[10^{-2}]$	$\tilde{\mathcal{R}}_{yy}$	$\tilde{\mathcal{R}}_{yz}$ $[10^{-2}]$	$\tilde{\mathcal{R}}_{zz}$	$\tilde{\mathcal{F}}_x$ $[10^{-2}]$	$\tilde{\mathcal{F}}_y$ $[10^{-2}]$	$\tilde{\mathcal{F}}_z$	$\tilde{\mathcal{Q}}$
Z	0°	0.00	0.00	87	0.114	0.083	−0.134	0.113	0.139	0.365	−0.169	0.105	0.286	0.333
A1	0°	0.04	0.06	91	0.119	−0.013	0.025	0.119	−0.145	0.412	−0.025	−0.178	0.329	0.381
A2	0°	0.16	0.11	92	0.123	−0.030	−0.117	0.123	−0.088	0.419	−0.166	−0.095	0.333	0.386
A3	0°	0.36	0.16	95	0.127	0.009	0.006	0.128	−0.015	0.455	0.051	−0.098	0.362	0.417
A4	0°	1.00	0.26	97	0.131	−0.021	0.022	0.131	−0.043	0.481	0.049	−0.040	0.382	0.436
A5	0°	1.44	0.31	100	0.135	0.005	0.049	0.136	0.068	0.511	0.047	0.044	0.406	0.462
A6	0°	2.56	0.39	103	0.143	0.032	0.070	0.144	−0.142	0.548	0.128	−0.191	0.428	0.480
A7•	0°	4.00	0.47	107	0.161	−0.009	−0.312	0.158	−0.085	0.593	−0.275	−0.168	0.499	0.725
A8	0°	12.96	0.76	120	0.174	0.057	−0.670	0.175	0.053	0.795	−0.614	0.048	0.611	0.656
A9	0°	100	1.71	148	0.221	−0.132	−0.373	0.219	−0.524	1.285	−0.417	−0.379	0.984	1.021
A10	0°	400	3.29	154	0.225	−0.115	−0.609	0.217	−0.629	1.424	−0.735	−0.564	1.067	1.096
A11	0°	10000	10.79	235	0.252	0.016	0.295	0.254	−0.582	3.849	−0.005	−0.241	2.947	2.839
B1	15°	0.04	0.06	90	0.121	−0.045	−0.275	0.120	−1.211	0.400	−0.220	−1.301	0.316	0.367
B2	15°	0.16	0.11	90	0.118	−0.012	−0.173	0.121	−2.358	0.395	−0.188	−2.464	0.312	0.363
B3	15°	0.36	0.18	85	0.110	0.098	−0.504	0.117	−3.191	0.350	−0.650	−3.384	0.276	0.326
B4	15°	1.00	0.30	85	0.110	0.213	−0.947	0.122	−4.456	0.337	−1.152	−4.955	0.268	0.319
B5	15°	1.44	0.36	84	0.109	0.313	−1.106	0.123	−4.479	0.323	−1.459	−5.120	0.257	0.310
B6	15°	2.56	0.51	80	0.104	0.316	−1.313	0.119	−4.158	0.284	−1.875	−4.963	0.227	0.279
B7•	15°	4.00	0.62	81	0.111	0.214	−1.246	0.122	−3.931	0.288	−1.944	−5.176	0.243	0.357
B8	15°	5.76	0.75	81	0.110	0.190	−1.613	0.125	−3.797	0.278	−2.330	−5.123	0.223	0.279
B9	15°	10.24	0.99	82	0.119	−0.021	−1.421	0.127	−3.261	0.286	−2.112	−4.939	0.226	0.284
B10	15°	16	1.27	80	0.119	−0.030	−0.980	0.125	−2.528	0.261	−1.514	−4.997	0.200	0.256
B11	15°	100	1.73	146	0.447	1.485	29.507	0.258	−4.673	0.987	18.614	−10.961	0.657	0.760
B12	15°	400	1.71	296	1.988	3.467	201.160	0.615	−9.467	4.323	123.721	−23.260	2.725	2.650
C1	30°	0.04	0.06	89	0.116	0.022	−0.103	0.119	−2.333	0.390	−0.175	−2.492	0.310	0.362
C2	30°	0.16	0.12	86	0.110	0.093	−0.470	0.120	−3.776	0.352	−0.531	−4.210	0.283	0.336
C3	30°	0.36	0.19	80	0.099	0.277	−0.587	0.114	−4.365	0.289	−0.787	−5.068	0.234	0.286
C4	30°	1.00	0.34	74	0.091	0.561	−1.261	0.110	−4.293	0.232	−1.762	−5.499	0.191	0.244
C5	30°	1.44	0.42	72	0.088	0.597	−1.430	0.108	−3.892	0.214	−2.089	−5.415	0.177	0.230
C6	30°	2.56	0.58	70	0.088	0.531	−1.565	0.104	−3.263	0.200	−2.350	−5.005	0.163	0.217
C7•	30°	4.00	0.70	73	0.099	0.417	−1.223	0.112	−3.191	0.208	−2.463	−5.620	0.176	0.249
C8	30°	5.76	0.84	73	0.098	0.455	−1.177	0.108	−2.732	0.212	−2.413	−5.026	0.168	0.228
C9	30°	10.24	1.02	80	0.118	0.362	0.377	0.123	−2.702	0.262	−1.622	−5.732	0.196	0.266
C10•	30°	16	1.13	89	0.157	0.533	3.083	0.143	−2.810	0.331	−0.544	−6.472	0.240	0.369
C11•	30°	100	1.14	223	1.023	2.198	83.326	0.483	−7.129	2.419	28.885	−22.541	1.501	2.178
C12•	30°	400	1.24	407	3.727	5.181	297.646	1.053	−12.171	8.305	26.867	−52.942	5.341	11.037
C13•	30°	10000	3.18	798	13.330	8.958	722.547	2.298	−4.884	34.601	−717.873	−85.046	25.270	173.730
D1	45°	0.04	0.06	89	0.117	−0.021	0.063	0.122	−3.071	0.389	0.054	−3.341	0.311	0.365
D2	45°	0.16	0.12	82	0.101	0.157	−0.449	0.119	−4.722	0.305	−0.527	−5.426	0.247	0.301
D3	45°	0.36	0.20	75	0.089	0.405	−0.635	0.113	−4.609	0.239	−0.885	−5.861	0.196	0.249
D4	45°	1.00	0.39	65	0.075	0.705	−1.168	0.097	−3.566	0.165	−1.822	−5.472	0.138	0.187
D5	45°	1.44	0.47	64	0.074	0.755	−1.218	0.094	−3.145	0.158	−1.982	−5.180	0.130	0.180
D6	45°	2.56	0.65	62	0.075	0.735	−1.050	0.087	−2.470	0.144	−2.061	−4.689	0.116	0.166
D7•	45°	4.00	0.72	70	0.098	0.527	−0.058	0.105	−2.473	0.188	−1.131	−5.279	0.150	0.234
D8	45°	5.76	0.83	74	0.104	0.701	0.183	0.110	−2.450	0.215	−1.415	−5.606	0.160	0.228
D9	45°	10.24	0.89	91	0.152	0.816	2.599	0.152	−2.936	0.348	−0.114	−7.675	0.247	0.343
D10•	45°	16	0.95	107	0.218	0.937	8.224	0.184	−3.041	0.505	2.167	−9.218	0.354	0.554
D11•	45°	100	1.02	247	1.079	1.361	90.448	0.535	−5.660	3.209	24.256	−27.786	1.906	2.882
D12•	45°	400	1.17	432	3.277	1.797	300.328	0.994	−9.638	10.468	−25.959	−59.461	5.819	13.090
D13•	45°	10000	2.22	1143	24.515	6.300	1403.346	5.534	1.043	73.121	−4214.031	−253.095	76.100	715.106

Table C2: Summary of the DNS results continued. For normalizations see TableC1.

Run	ϑ	Ta $[10^6]$	Co	Re	$\tilde{\mathcal{R}}_{xx}$	$\tilde{\mathcal{R}}_{xy}$ $[10^{-2}]$	$\tilde{\mathcal{R}}_{xz}$ $[10^{-2}]$	$\tilde{\mathcal{R}}_{yy}$	$\tilde{\mathcal{R}}_{yz}$ $[10^{-2}]$	$\tilde{\mathcal{R}}_{zz}$	$\tilde{\mathcal{F}}_x$ $[10^{-2}]$	$\tilde{\mathcal{F}}_y$ $[10^{-2}]$	$\tilde{\mathcal{F}}_z$	$\tilde{\mathcal{Q}}$
E1	60°	0.04	0.06	87	0.112	0.034	−0.115	0.120	−3.451	0.362	−0.107	−3.774	0.288	0.339
E2	60°	0.16	0.13	76	0.091	0.180	−0.280	0.113	−4.469	0.253	−0.398	−5.385	0.205	0.254
E3	60°	0.36	0.22	69	0.078	0.437	−0.514	0.106	−4.202	0.192	−0.792	−5.826	0.159	0.208
E4	60°	1.00	0.43	59	0.063	0.640	−0.714	0.089	−2.796	0.128	−1.252	−5.021	0.105	0.151
E5	60°	1.44	0.53	58	0.062	0.697	−0.670	0.081	−2.293	0.118	−1.313	−4.488	0.096	0.139
E6	60°	2.56	0.68	60	0.068	0.721	−0.379	0.085	−1.930	0.128	−1.087	−4.602	0.096	0.146
E7•	60°	4.00	0.77	66	0.084	0.901	−0.257	0.096	−1.722	0.159	−1.057	−4.858	0.120	0.200
E8	60°	5.76	0.84	72	0.099	0.862	0.070	0.112	−1.677	0.204	−0.658	−5.227	0.143	0.213
E9	60°	10.24	0.92	89	0.138	0.929	0.437	0.155	−1.790	0.326	0.112	−6.615	0.219	0.317
E10	60°	16.00	1.01	101	0.182	1.256	1.335	0.181	−1.271	0.436	0.261	−6.841	0.278	0.386
F1	75°	0.04	0.06	85	0.108	0.015	0.001	0.120	−3.963	0.347	−0.028	−4.396	0.278	0.331
F2	75°	0.16	0.13	75	0.089	0.089	−0.175	0.114	−4.675	0.246	−0.187	−5.806	0.201	0.253
F3	75°	0.36	0.23	66	0.071	0.287	−0.332	0.104	−4.106	0.171	−0.493	−5.951	0.143	0.193
F4	75°	1.00	0.44	57	0.055	0.467	−0.366	0.086	−2.566	0.115	−0.674	−5.068	0.094	0.140
F5	75°	1.44	0.56	54	0.051	0.544	−0.327	0.078	−1.966	0.100	−0.659	−4.454	0.079	0.123
F6	75°	2.56	0.71	57	0.059	0.697	−0.328	0.083	−1.418	0.113	−0.550	−3.953	0.083	0.128
F7•	75°	4.00	0.83	61	0.068	1.006	−0.626	0.092	−1.061	0.131	−0.722	−3.809	0.092	0.159
F8	75°	5.76	0.91	67	0.082	1.364	−0.582	0.108	−0.836	0.162	−0.572	−3.556	0.103	0.138
F9	75°	12.96	1.06	86	0.134	1.513	−0.810	0.158	−0.715	0.296	0.201	−4.813	0.177	0.275
G1	90°	0.04	0.06	85	0.108	0.015	−0.025	0.120	−3.925	0.347	−0.046	−4.319	0.279	0.332
G2	90°	0.16	0.14	75	0.087	0.010	−0.064	0.114	−4.725	0.240	−0.073	−5.925	0.197	0.250
G3	90°	0.36	0.23	66	0.069	−0.012	0.004	0.107	−4.144	0.168	−0.008	−6.277	0.141	0.192
G4	90°	1.00	0.44	58	0.054	0.096	−0.121	0.090	−2.500	0.120	−0.265	−5.076	0.095	0.141
G5	90°	1.44	0.57	53	0.045	0.004	0.018	0.082	−1.870	0.098	0.028	−4.503	0.075	0.119
G6	90°	2.56	0.86	47	0.024	0.065	−0.031	0.088	−0.645	0.062	−0.049	−2.702	0.041	0.075
G7	90°	4.00	1.08	47	0.018	0.029	0.026	0.100	−0.271	0.058	−0.077	−1.572	0.031	0.060
G8•	90°	4.00	1.02	50	0.022	−0.013	0.056	0.103	−0.490	0.069	0.106	−2.211	0.038	0.078

Table C3: Summary of the DNS results with different Rayleigh numbers, $\mathrm{Pr} = 1$. The non–primed runs are non–rotating, while for the primed runs $\mathrm{Ta} = 10^6$ and $\vartheta = 0°$. For normalizations see Table C1. The grid resolutions are 64^3 (R1–2), 128^3 (R3–4), 256^3 (R5), and 512^3 (R6).

Run	Ra $[10^6]$	Co	Re	$\tilde{\mathcal{R}}_{xx}$	$\tilde{\mathcal{R}}_{xy}$ $[10^{-2}]$	$\tilde{\mathcal{R}}_{xz}$ $[10^{-2}]$	$\tilde{\mathcal{R}}_{yy}$	$\tilde{\mathcal{R}}_{yz}$ $[10^{-2}]$	$\tilde{\mathcal{R}}_{zz}$	$\tilde{\mathcal{F}}_x$ $[10^{-2}]$	$\tilde{\mathcal{F}}_y$ $[10^{-2}]$	$\tilde{\mathcal{F}}_z$	$\tilde{\mathcal{Q}}$
R1	0.25	0	68	0.126	−0.029	0.018	0.128	0.041	0.480	0.064	0.063	0.403	0.498
R2	1	0	128	0.123	0.032	−0.209	0.124	0.001	0.395	−0.331	0.015	0.317	0.411
R3	4	0	259	0.131	−0.014	0.115	0.131	−0.090	0.399	0.205	−0.053	0.303	0.391
R4	10	0	460	0.155	−0.018	0.273	0.155	−0.178	0.525	0.307	−0.163	0.391	0.485
R5	25	0	772	0.171	0.072	−0.250	0.172	−0.006	0.598	−0.308	−0.148	0.440	0.533
R6	200	0	2358	0.188	−0.035	0.209	0.189	−0.340	0.698	0.207	−0.313	0.506	0.586
R1'	1	0.2	128	0.127	0.060	−0.126	0.124	0.034	0.400	−0.007	0.026	0.321	0.413
R2'	4	0.09	289	0.154	−0.024	0.036	0.151	−0.313	0.520	0.017	−0.273	0.395	0.494
R3'	25	0.03	764	0.164	0.013	−0.087	0.165	−0.148	0.593	−0.062	−0.148	0.438	0.528

Chandrasekhar, S. 1961, Hydrodynamic and hydromagnetic stability (Clarendon Press, Oxford)
Garaud, P. & Ogilvie, G. I. 2005, Journal of Fluid Mechanics, 530, 145
Garaud, P., Ogilvie, G. I., Miller, N., & Stellmach, S. 2010, MNRAS , 407, 2451
Ghizaru, M., Charbonneau, P., & Smolarkiewicz, P. K. 2010, ApJ , 715, L133
Käpylä, P. J. 2011, Astronomische Nachrichten, 332, 43
Käpylä, P. J. & Brandenburg, A. 2008, Astron. Astrophys., 488, 9
Käpylä, P. J., Korpi, M. J., & Tuominen, I. 2004, Astron. Astrophys., 422, 793

Table C4: Summary of the DNS results with box aspect ratios $\Gamma = 4$ and 0.75 (last line); $\mathrm{Ra} = 3 \cdot 10^5$, $\mathrm{Pr} = 0.6$, $\mathrm{Ta} = 4 \cdot 10^6$. The grid resolution is $128^2 \times 256$ and $144^2 \times 108$, respectively. For normalizations see Table C1. For d the horizontal extent was used as in the dimensionless numbers, too. Viscous heating is included throughout.

ϑ	Co	Re	$\tilde{\mathcal{R}}_{xx}$	$\tilde{\mathcal{R}}_{xy}[10^{-2}]$	$\tilde{\mathcal{R}}_{xz}[10^{-2}]$	$\tilde{\mathcal{R}}_{yy}$	$\tilde{\mathcal{R}}_{yz}[10^{-2}]$	$\tilde{\mathcal{R}}_{zz}$	$\tilde{\mathcal{F}}_x[10^{-2}]$	$\tilde{\mathcal{F}}_y[10^{-2}]$	$\tilde{\mathcal{F}}_z$	$\tilde{\mathcal{Q}}$
0°	0.627	81	0.125	−0.021	0.194	0.124	0.080	0.267	0.251	0.087	0.227	0.389
15°	0.657	77	0.119	0.229	−1.543	0.117	−1.612	0.233	−2.258	−2.420	0.200	0.345
30°	0.739	69	0.103	0.669	−2.226	0.099	−2.094	0.169	−3.373	−3.560	0.144	0.249
45°	0.785	65	0.097	0.838	−0.923	0.090	−1.768	0.142	−2.393	−3.917	0.115	0.208
60°	0.761	67	0.100	0.938	−0.534	0.104	−1.645	0.146	−1.700	−4.480	0.109	0.217
75°	0.837	60	0.080	1.165	−0.399	0.095	−0.800	0.115	−1.029	−3.627	0.079	0.169
90°	1.004	50	0.005	0.068	−0.007	0.170	0.037	0.026	−0.023	−1.598	0.014	0.045
45°	0.733	69	0.086	0.679	−0.430	0.103	−2.813	0.189	−1.703	−6.069	0.148	0.226

Käpylä, P. J., Mantere, M. J., & Brandenburg, A. 2012, ApJ , 755, L22

Käpylä, P. J., Mantere, M. J., Guerrero, G., Brandenburg, A., & Chatterjee, P. 2011, Astron. Astrophys., 531, A162

Kichatinov, L. L. & Rüdiger, G. 1993, Astron. Astrophys., 276, 96

Kitchatinov, L. L. & Rüdiger, G. 2005, Astronomische Nachrichten, 326, 379

Krause, F. & Rädler, K. 1980, Mean–field magnetohydrodynamics and dynamo theory (Pergamon Press Ltd., Oxford)

Lasdon, L., Waren, A., Jain, A., & Ratner, M. 1978, ACM Transactions on Mathematical Software, 4, 34

Liljeström, A. J., Korpi, M. J., Käpylä, P. J., Brandenburg, A., & Lyra, W. 2009, Astronomische Nachrichten, 330, 92

Miesch, M. S., Brun, A. S., & Toomre, J. 2006, ApJ , 641, 618

Miesch, M. S. & Toomre, J. 2009, Annual Review of Fluid Mechanics, 41, 317

Miller, N. & Garaud, P. 2007, in American Institute of Physics Conference Series, Vol. 948, Unsolved Problems in Stellar Physics: A Conference in Honor of Douglas Gough, ed. R. J. Stancliffe, G. Houdek, R. G. Martin, & C. A. Tout, 165–169

Moffatt, H. K. 1978, Magnetic field generation in electrically conducting fluids

Ogilvie, G. I. 2003, MNRAS , 340, 969

Pulkkinen, P., Tuominen, I., Brandenburg, A., Nordlund, A., & Stein, R. F. 1993, Astron. Astrophys., 267, 265

Rieutord, M., Brandenburg, A., Mangeney, A., & Drossart, P. 1994, Astron. Astrophys., 286, 471

Rüdiger, G. 1989, Differential rotation and stellar convection. Sun and the solar stars (Akademie Verlag, Berlin)

Rüdiger, G., Egorov, P., Kitchatinov, L. L., & Küker, M. 2005a, Astron. Astrophys., 431, 345

Rüdiger, G., Egorov, P., & Ziegler, U. 2005b, Astronomische Nachrichten, 326, 315

Rüdiger, G. & Hollerbach, R. 2004, The magnetic universe : geophysical and astrophysical dynamo theory (Wiley-VCH)

Snellman, J. E., Brandenburg, A., Käpylä, P. J., & Mantere, M. J. 2012a, Astronomische Nachrichten, 333, 78

Snellman, J. E., Käpylä, P. J., Korpi, M. J., & Liljeström, A. J. 2009, Astron. Astrophys., 505, 955

Snellman, J. E., Rheinhardt, M., Käpylä, P. J., Mantere, M. J., & Brandenburg, A. 2012b, Physica Scripta, 86, 018406

Spiegel, E. A. & Veronis, G. 1960, ApJ , 131, 442

Warnecke, J., Käpylä, P. J., Mantere, M. J., & Brandenburg, A. 2013, ApJ , 778, 141

Yamaguchi, S. 1963, PASJ , 15, 412

Xiong, D.-R. 1989, Astron. Astrophys., 209, 126

Xiong, D. R., Cheng, Q. L., & Deng, L. 1997, ApJS , 108, 529